



Proposal and energy, exergy, economic, and environmental analyses of a novel combined cooling and power (CCP) system

Mohsen Fallah¹ · Arvin Sohrabi² · Narges H. Mokarram³

Received: 28 September 2022 / Accepted: 18 July 2023 / Published online: 5 August 2023
© The Author(s), under exclusive licence to The Brazilian Society of Mechanical Sciences and Engineering 2023

Abstract

This study proposes a new combined cooling and power generation system for sustainable heat recovery from diesel engines used in industrial applications. In this regard, a novel high-temperature Kalina cycle integrated with an organic Rankin cycle and two-stage vapor compression refrigeration system is proposed and investigated to recover the waste heat from a 320 kW diesel engine fully. The exhaust gas as the heat source provides thermal energy to run the combined cycle. A MATLAB simulation code is written to assess and investigate the proposed system's energy, exergy, economic, and environmental (4E) analyses. Also, a parametric study is carried out to reveal the effects of different parameters on four thermodynamic parameters (power production, energy and exergy efficiencies, and exergy destruction) and four thermo-economic parameters (cost rate, LCOE, NPV, and payback period). Results show that utilizing this combined system will lead to producing 60 kW more power. This is equivalent to almost 19% more power compared to the stand-alone diesel engine. Also, the exergy efficiency of the system is 58.3%. The economic results show that the generated power costs 0.06 \$/kWh (6.12 cent/kWh). Based on the environmental study, the system prevents the emission of 35.3 kg of carbon dioxide per h.

Keywords Cooling · Diesel engine · Kalina · Organic rankine cycle (ORC) · Vapor compression refrigeration (VCR) · Cost rate

List of Symbols

c	Area (m ²)
AP	Annual profit
C_r	Compressor ratio
\dot{C}	Cost rate (\$ s ⁻¹)
\dot{C}_P	Product cost rate
\dot{C}_{CI}	Capital investment cost rate
\dot{C}_{OM}	Operating and maintenance cost rate
\dot{C}_F	Fuel cost rate
c_{se}	Unit price of electricity (\$/kWh)
CRF	Capital recovery factor
C	Compressor

CD	Condenser
DPP	Dynamic period payback (year)
e^0	Standard chemical exergy (kJ kmol ⁻¹ K ⁻¹)
e_{ph}	Physical exergy flow
e_{ch}	Chemical exergy flow
\dot{E}	Exergy rate (kW)
Ev	Evaporator
F	Flash Chamber
G	Electrical generator
h	Specific enthalpy (kJ kg ⁻¹)
i	Nominal interest rate
IRR	Internal rate of return
KC	Kalina Cycle
LCOE	Levelized cost of energy (\$/kWh)
\dot{m}	Mass flow rate (kg s ⁻¹)
MOIC	Multiple of investment capital
MW	Molecular weight (kg kmol ⁻¹)
MX	Mixing chamber
n	System lifetime (year)
N	Operational hours in a year (h)
NPV	Net present value (k\$)
ORC	Organic rankine cycle
P	Pressure (kPa)
PEC	Purchased equipment cost (k\$)

Technical Editor: Monica Carvalho.

✉ Mohsen Fallah
mfallah@azaruniv.ac.ir

¹ Department of Mechanical Engineering, Azarbaijan Shahid Madani University, Tabriz, Iran

² School of Mechanical Engineering, Beijing Institute of Technology, Beijing 100081, China

³ Division of Systems, Power and Energy, School of Engineering, University of Glasgow, Glasgow, UK

Pu	Pump
\dot{Q}	Heat rate (kW)
Re	Recuperator
s	Specific entropy ($\text{kJ kg}^{-1} \text{K}^{-1}$)
sg	Steam generator
T	Temperature ($^{\circ}\text{C}$)
Tu	Turbine
TV	Throttling valve
TCI	Total capital investment (k\$)
ΔT_{in}	Logarithmic mean temperature difference (K)
U	Overall heat transfer coefficient ($\text{W m}^{-2} \text{K}^{-1}$)
VCR	Vapor Compression Refrigeration
\dot{W}	Power (kW)
x	Ammonia concentration in ammonia-water solution
$Y_i, i = 1 : 3$	Constant coefficients of heat exchanger cost functions

Greek symbols

ϕ	Operating and maintenance factor (%)
ΔT_{in}	Logarithmic mean temperature difference
τ	System annual operating hours
ε	Exergy efficiency (%)
η	Energy efficiency (%)
$\eta_{\text{is,c}}$	Isentropic efficiency of compressor (%)

Subscripts

0	Ambient
1, 2, 3, ...,	State points
cyc	Cycle
F	Fuel (cost rate)
in	Inlet
HX	Heat exchanger
out	Outlet
Pu	Pump
tot	Total
wf	Working fluid

1 Introduction

Researchers try to find ways to reduce harmful emissions from industrial and commercial activities. Environmental pollution and decreased resources available are the results of poor management in using energy resources for a long time. Concerns about environmental problems have increased due to the general rise in world temperature as a greenhouse effect. It is the reason to use a more efficient system as a basic solution provided by researchers [1].

Internal engine combustions (ICEs) consume approximately 60–70% of the total fossil fuel of an industrial country, 40–50% of which is used by automotive ICEs.

However, about 75% of the total fuel combustion thermal energy in automotive ICEs will be wasted by the exhaust and engine coolant, which leads to an emission problem [2, 3].

Different thermodynamics cycles are proposed and designed for waste heat recovery (WHR) to increase the efficiency of the power generation cycles, including the Sterling cycle, carbon dioxide cycles (CDC), Kalina cycle (KC), organic Rankine cycle (ORC) (works for medium to low-temperature applications), air bottoming cycles (ABC) (works for high-temperature applications), and absorption refrigeration cycle [4–7].

The first Kalina cycle was proposed by Leibowitz and Kalina [8]. They designed a 3 MW Kalina cycle and showed that a single-pressure design with the same pick temperature led to more power production, up to 25%, compared to an ORC one. Due to its high potential to recover waste heat, the Kalina cycle has been used in different systems. Such a potential comes from the non-iso-thermal evaporation and condensation processes of the zeotropic ammonia-water mixture, making a tight thermal match between two high and low sources, subsequently, a high thermal efficiency [9]. A waste heat recovery system, including a heating system and a prototype heat-driven ejector refrigeration cycle to recover the waste heat of small and mid-sized maritime combustion engines (100–250 kW) was proposed by Butrymowicz et al. [10] and experimentally investigated. Using such a heat recovery system could produce up to 30 kW of cooling by consuming 75 kW of the refrigeration system from the flue gas heat source.

Ouyang et al. [11] proposed a combined evaluation method based on thermodynamics, economics, and environment to study a dual-pressure ORC as the exhaust gas waste heat recovery system in marine engines. A parametric study with six commonly used working fluids and multi-objective optimization was conducted in their studies. The optimum condition led to obtaining an exergy efficiency of 60.24%, while the production cost of electricity was 0.167 \$/kWh. Acikkalp et al. [12] investigated a trigeneration system for an industrial application based on conventional and advanced exergy analyses. They showed that the interconnections among the components were relatively high. Bo et al. [13] designed an auxiliary tri-generation cycle that included a Kalina cycle, an ejector-booster refrigeration cycle, and a desalination unit production to recover the waste heat from a ship engine. They conducted thermodynamic and exergo-economic analyses as well as a parametric analysis and genetic algorithm optimization to evaluate the proposed system.

Singh et al. [14] studied a Brayton-Rankine-Kalina combined cycle, including a natural gas-fired Brayton-Rankine power plant in New Delhi, India, and the geothermal Kalina power plant in Husavik, Iceland. They performed a thermo-economic analysis and optimization using the SPECOC¹ method to calculate each node's cost per unit exergy and thermo-economic variables for different components in the cycle. It was concluded that the exergy loss cost of steam turbines, HRSGs, combustion chambers, compressors, recuperators, and ammonia-water evaporators was higher than others. Therefore, their performances had to be improved. Invernizzi et al. [15] compared waste heat recovery Kalina and ORC systems from two Diesel engines with an electric capacity of 8900 kWe. The maximum net electric power of the two cycles was 1615 kW and 1603 kW for the Kalina and the ORC cycle, respectively. The waste heat of the 8S90ME-C10.2 two-stroke low-speed diesel engine has been recovered by Feng et al. [16]. They performed a thermodynamic analysis using MATLAB-REFPROP to compare the basic diesel system with the proposed combined cycle system coupling SCBC² and KC cycles. It was shown that the combined supercritical carbon dioxide Brayton cycle and Kalina cycle reduced the average annual fuel consumption of marine engines and the EEDI (Energy Efficiency Design Index) factor by 16.62% and 15.01%, respectively.

Hua et al. [17] conducted energy and exergy analyses and optimization of the boiler evaporation process of a waste heat recovery Kalina cycle. They presented that exergy and power recovery efficiencies were 18.32% and 48.32% if high and low-temperature sources were at 300 °C and 25 °C, respectively. Ranjbar et al. [18] performed an exergoeconomic analysis of a power cycle based on the Diesel-Kalina cycle, as well as an assessment of system responses to changes in different parameters. The results showed that 21.74 kW of power was produced from waste heat recovery, which is remarkable compared to 98.9 kW of engine power. Baldi et al. [19] proposed a new method to calculate the available amount of installation of waste heat recovery systems for marine applications. The results showed that such a method leads to a reduction in fuel consumption by up to 4–16% and makes the system profitable in 2 to 5 years. Larsen et al. [20] studied a split-Kalina cycle with and without reheat and compared it with the conventional Kalina cycle. The reheated version was able to produce 11.4% more power. The optimizing procedure shows that the turbine exhaust pressure and the boiler inlet temperature are the most important factors in maximizing cycle efficiency.

The experimenting of a prototype heat recovery system designed for small and medium-sized marine combustion engines with a nominal load of 100–250 kW was provided by Butrymowicz et al. [10]. The refrigeration system was designed to provide up to 30 kW of cold while using 75 kW of heat extracted from flue gases. Additionally, the waste heat recovery system offered around 60 kW of heat collected from the jacket water cooling of the engine block and was used for tap water and space heating. A system that combined cooling, heating, and power generating was suggested by Najafi et al. [21]. For those purposes, the engine-rejected heat recovery system included a domestic water heater (DWH), an organic Rankine cycle (ORC), and an ejector refrigeration cycle (ERC). To power the bottoming cycles, the diesel engine was supplied with various fuels and biofuels. The generated biodiesel was fed into the diesel engine at different engine speeds and loads in order to assess the system's efficiency from an energy and exergy perspective. According to the data, using biodiesel and diesel mixed as fuel instead of pure diesel significantly improved energy efficiency.

The steam Rankine cycle (RC), organic Rankine cycle (ORC), and absorption refrigeration cycle (ARC) were the three sub-cycles proposed as the waste heat recovery system from waste heat from the jacket cooling water and exhaust gas (EG) by He et al. [22]. The proposed waste heat recovery system (WHRS) was assessed for the thermodynamic performance. The impact of additional factors, such as evaporation pressure, superheat, and engine load, was also examined. In comparison to WHRSs based on single RC and dual loop ORC, the designed WHRS can output 7620 kW of electricity and 2940 kW of cooling energy under the engine's rated operating conditions. Yu et al. [23] proposed the recovery of waste heat from the engine using a supercritical CO₂ (S-CO₂) power cycle coupled with a transcritical CO₂ (T-CO₂) refrigeration cycle to provide a substitute for the vapor absorption cooling system. The S-CO₂ in this system absorbed heat from exhaust gases, and the power produced in the expander was utilized to power the compressors in both the S-CO₂ power cycle and the T-CO₂ refrigeration cycle. According to the findings, the idea of the S-CO₂/T-CO₂ combined cycle using a single cooler offered comparable performance and was thermodynamically viable.

Zhao et al. [24] used a transcritical-subcritical parallel organic Rankine cycle based on zeotropic mixtures to recover engine waste heat. Three design parameters were examined together with energy and exergy assessments. The findings showed that system performance initially increased and then decreased for each turbine inlet temperature of the high-pressure branch. Also, the net power output initially increased and then decreased with changes in the evaporation temperature of the low-pressure branch. Xiao et al. [25] proposed a cogeneration of electrical power and freshwater

¹ Specific Exergy Costing.

² supercritical carbon dioxide Brayton cycle.

to recover the waste heat of a diesel engine. Exhaust gas energy was utilized in the Kalina cycle to produce electricity, while jacket water energy was used in the HDH system to produce freshwater. The multi-objective optimization findings demonstrated an increase in thermal and exergy efficiency of 1.8% and 1.52%, respectively, compared to the base case values. The sum unit cost of the product (SUCP) value was also decreased by 0.94 \$/GJ.

A marine engine's waste heat recovery system was modeled by He et al. [26] and its performance was compared to that of WHRSs based on single steam Rankine cycles (SSRC) and dual pressure organic Rankine cycles (DPORC). The findings indicated that the suggested method might increase engine thermal efficiency by 4.42% while reducing fuel consumption by 9322 tonnes annually at a 100% engine load. At the same time, 2.68% and 3.42% more thermal efficiency may be achieved by a WHRS based on an SSRC and DPORC, respectively. Feng et al. [27] suggested a waste heat recovery method that coupled the supercritical carbon dioxide Brayton cycle power generation system with the Kalina cycle power generation system under as bottoming cycles of a low-speed marine diesel engine. The energy efficiency design index for the ship and the multi-objective optimization for improving the diesel engine and the combined power generation system were conducted. The results indicated that the yearly fuel consumption and the Energy Efficiency Design Index decreased to 16.62% and 15.01%, respectively.

Based on the reviewed literature, the proposed system in this study has not been studied before. Because of the higher waste thermal energy, the aim of this study is to fully recover the wasted heat of an exhaust gas source to produce the required power and cooling load of an industrial building. Since using one bottoming cycle may not be enough to recover the entire waste heat, a low-temperature cycle should be coupled to the system as well. Moreover, generating power from a waste heat source is always encouraging to run a utility such as a refrigeration cycle with more freedom. Another important aspect of using a waste heat source to generate power is that it is always associated with saving fuel and releasing pollutants, such as carbon dioxide, into the atmosphere.

To fill these gaps, the novel combined cycle includes a high-temperature Kalina cycle and a low-temperature ORC to generate power from the exhaust gas of a diesel engine, coupled with a two-stage VCR system that provides constant cool air is proposed. Also, to meet the demands of a comprehensive assessment [28, 29], this study investigates the proposed system based on energy, exergy, economic, and environmental viewpoints. A simulation code in MATLAB is developed to model the system to achieve the mentioned goals. Here, NIST23 (REFPROP) [30] is utilized to obtain the thermophysical properties of the streams.

Table 1 Model and properties of the used Diesel Engine

Characteristic	Value
Model name	C13 ACERT-DE400E0
Nominal capacity	400 kVA
Power factor	0.8
Generated power	320 kW
Fuel consumption	83.5 L/hr
Exhaust gas temperature	529.2 °C
Exhaust gas flow rate	62.8 m ³ /min (0.447 kg/s)

2 System description

To investigate the possibility of generating heat using waste heat sources, the heat source in this study is the exhaust gas that exits from a real diesel engine. The general data of the considered engine, besides the required information, are listed in Table 1 [31]. This engine can produce 400 kVA power with a power factor equal to 0.8, resulting in 320 kW net generated power at its full-load operation. Moreover, the compounds of a diesel engine exhaust gas are obtained from Ref. [32] which is: $N_2=0.7642$, $O_2=0.0948$, $CO_2=0.0756$, and $H_2O=0.0654$.

The exhaust gas of the engine is then used for further power generation. First, it enters a high-temperature Kalina cycle (KC). Then it is driven into an organic Rankine cycle (ORC), which recovers the remaining available heat in the exhaust gas, decreasing its temperature to the dew point limit. Producing remarkable power from a waste source enables us to use a portion of it for other power-consuming facilities. Hence, an industrial refrigeration (air cooling) system based on the two-stage vapor compression refrigeration (VCR) cycle with a flash chamber is coupled to the two cycles above-mentioned to provide the required cooling load. The power needed for the compressors of the refrigeration cycle is provided by the KC and the ORC. This cycle is designed in a way that shares a common condenser with the ORC. This decision leads to a lower capital investment since two heat exchangers merge into one.

A schematic of the proposed configuration is depicted in Fig. 1. Here, the hot exhaust gas from the diesel engine stack (stream 33) enters the KC steam generator, producing high-temperature and high-pressure steam from the water/ammonia mixture (stream 1). After expansion in the KC turbine, the superheated mixture (stream 2) enters the two internal heat exchangers (recuperators 1 and 2) to preheat the mixture in the inlet of the second condenser and the steam generator, respectively. Also, after the low-pressure pump divides into two streams, a portion goes to the high second condenser (stream 8), and the other (stream 9) is first preheated and then enters the flash separator. Saturated liquid from the separator (stream 12) is

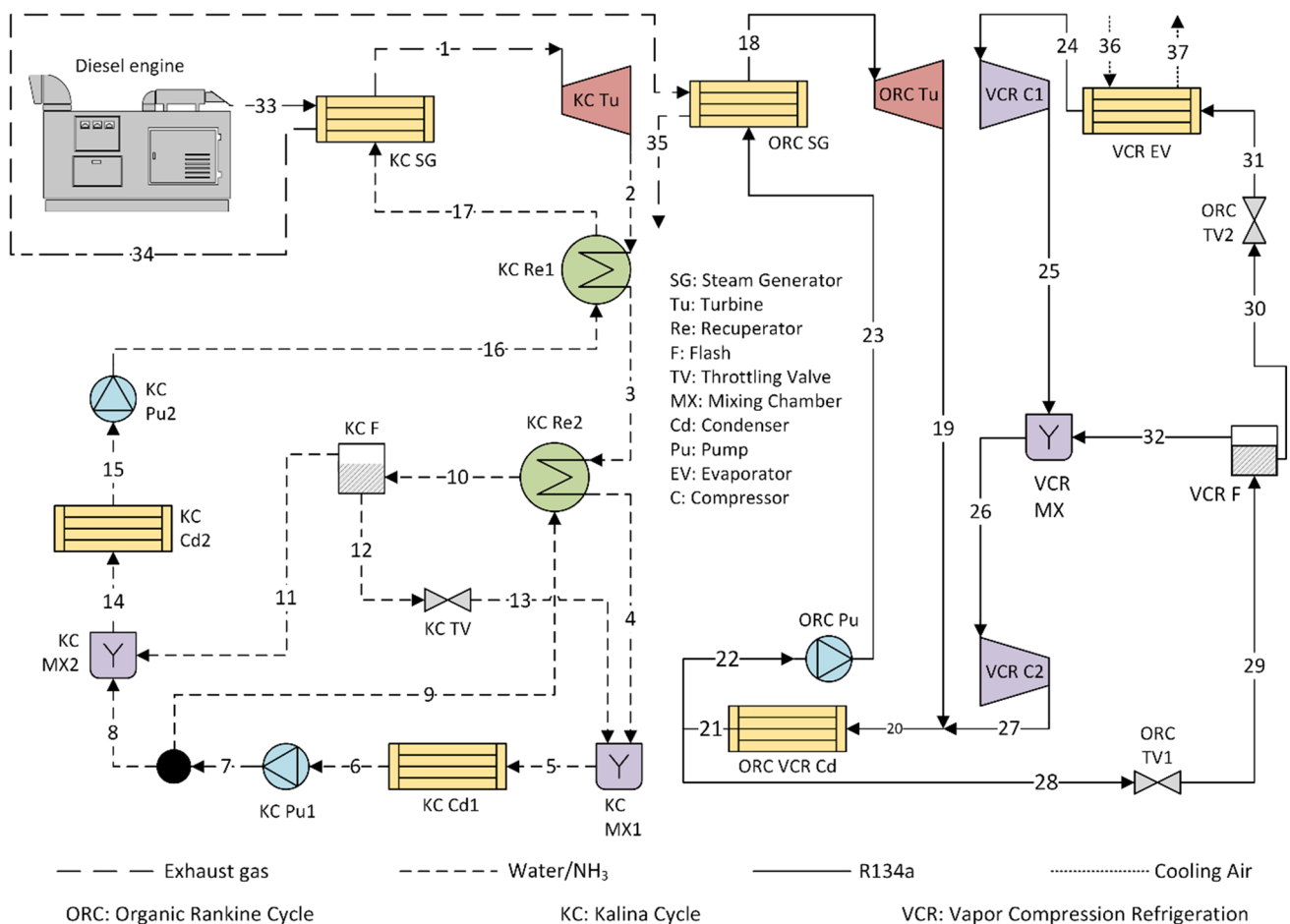


Fig. 1 Schematic figure of Kalina-ORC-VCR power and refrigeration combined cycle working with Diesel waste heat

expanded in a throttling valve and mixed with the outlet stream from the second recuperator (stream 4).

Moreover, saturated steam (stream 11) exits the separator and mixes with low-pressure subcooled liquid. After cooling in the second condenser, the stream is pressurized in the second pump. Its outlet (stream 16) is preheated and driven into the steam generator.

The remaining available heat in the exhaust gas recovers in the ORC steam generator (stream 34) and cools to the dew point limit. This heat exchanger produces a low-temperature and low-pressure steam from the working fluid, which is R134a in the current study. The exiting steam from the ORC turbine (stream 19) is mixed with the VCR compressor outlet (stream 27) to lose the excess heat in the condenser. After the condenser, the stream is again divided into two streams to feed both ORC and VCR. The ORC condensate (stream 22) enters the pump and the ORC steam generator, respectively. The VCR system, as seen, is a dual-stage type containing a flash intercooler between the two pressure stages. The condensed fluid (stream 28)

loses its pressure in the throttling valve, then enters the flash intercooler, where the steam and liquid are separated.

The steam (stream 32) combines with the low-pressure compressor outlet (stream 25) and enters the high-pressure compressor (stream 26). The saturated liquid (stream 30), on the other hand, reaches the evaporator pressure through a throttling valve and enters the evaporator (stream 31) to absorb heat from the air that enters the evaporator (stream 36) and deliver cold air to the room (stream 37).

It should be noted that the cooling water streams of the condensers and the electric generators are not shown in Fig. 1 to prevent overcrowding.

3 Methodology

Throughout the study, some parameters are considered constant based on the operating conditions. These parameters are listed in Table 2. To prevent the formation of acid due to the condensation in the exhaust gas side of heat exchangers,

Table 2 Initial thermodynamic assumption of simulation

Parameter	Value		Value
Ambient temperature (°C)	30 ^a	Other heat exchangers pinch point temperature (°C)	10 ^b
Ambient pressure (bar)	1.013 ^a	Pressure drop within KC steam generator (%)	8 ^d
Heat source minimum temperature (°C)	105 ^a	KC turbine inlet Ammonia concentration	0.8 ^b
Heat source pressure (bar)	1.013 ^a	KC turbine inlet temperature (°C)	480 ^d
Cooling water inlet temperature (°C)	20 ^b	KC turbine inlet pressure (bar)	140 ^d
Cooling water outlet temperature (°C)	30 ^b	ORC turbine inlet pressure (bar)	43 ^e
Cooling water pressure (bar)	1.013 ^b	VCR evaporator inlet temperature (°C)	4 ^c
Pump isentropic efficiency (%)	70 ^b	VCR evaporator outlet temperature (°C)	-3 ^c
Turbine isentropic efficiency (%)	85 ^b	VCR evaporator mass flow rate (kg/s)	3 ^c
Generator efficiency (%)	98 ^b	Superheating degree in VCR evaporator (°C)	5 ^c
Compressor efficiency (%)	0.65 ^c	VCR flash intercooler Pressure (bar)	4 ^c
Condenser pinch point temperature (°C)	7 ^b		

a [42], b [41], c [36], d [35], e [37]

the lower limit of its temperature is set to 90 °C [33, 34]. Also, the steam quality at the turbine outlet, both in the KC and the ORC, should not be lower than 0.9 to avoid corrosion in the expander's final stages [35]. Generators coupled to the turbines provide the required power for pumps and compressors.

Since the VCR provides cold air for industrial refrigeration applications, it is assumed that its working h is equal to that of the power-producing sections. In addition, all components of the considered structure operate in steady-state conditions. Also, the potential and kinetic energies of the streams do not change.

The thermodynamic properties of the streams are obtained from the REFPROP 9 library [30], which is coupled with MATLAB. It should be noted that for heat source streams and water-ammonia mixtures, the concentration (mass fraction) of each component must be taken into account to calculate the unknown parameters of the streams correctly. This is important for calculating the enthalpy and entropy values that are required in energy and exergy analyses.

3.1 Energy and exergy analysis

Each component is supposed to be a control volume for the thermodynamic modeling of the considered structure. The mass and energy balances for each control volume are given as Eqs. (1) and (2) [38]:

$$\sum \dot{m}_{in} = \sum \dot{m}_{out} \quad (1)$$

$$\sum \dot{m}_{in} h_{in} + \dot{Q} = \sum \dot{m}_{out} h_{out} + \dot{W} \quad (2)$$

The energy efficiency of the KC and the ORC is obtained as follows [38]:

$$\eta_{KC,ORC} = \frac{\dot{W}_{net}}{\dot{Q}_{in}} \quad (3)$$

\dot{Q}_{in} is the recovered heat from the exhaust gas in steam generators of Kalina and organic Rankine cycles [39].

$$\dot{Q}_{in} = \dot{m}_{hf} (h_{hf,in}^{SG} - h_{hf,out}^{SG}) \quad (4)$$

The produced power for either KC or ORC, \dot{W}_{net} , is calculated using Eqs. (5)-(8) [40]. It is noteworthy that since the required power of the pump is calculated as a negative value according to Eq. (7), the plus sign is used in Eq. (5)

$$\dot{W}_{net}^{KC,ORC} = \dot{W}_G^{KC,ORC} + \dot{W}_{Pu}^{KC,ORC} \quad (5)$$

$$\dot{W}_G^{KC,ORC} = \eta_G \dot{W}_{Tu} \quad (6)$$

$$\dot{W}_{Tu} = \dot{m}_{wf} (h_{wf,in}^{Tu} - h_{wf,out}^{Tu}) \quad (7)$$

$$\dot{W}_{Pu} = \dot{m}_{wf} (h_{wf,in}^{Pu} - h_{wf,out}^{Pu}) \quad (8)$$

Moreover, for the vapor compression refrigeration cycle, the coefficient of performance (COP) is defined as the absorbed heat in the evaporator divided by the required work in the compressors, as shown in Eqs. (9)-(11). Equation (10) is defined in a way that the value of \dot{Q}_{EV} remains positive.

$$COP = \frac{\dot{Q}_{EV}}{\dot{W}_C} \quad (9)$$

Table 3 Energy and exergy balances for the components of the proposed system

Component	Mass balance	Energy and exergy balances
KC SG	$\dot{m}_{17} + \dot{m}_{33} = \dot{m}_1 + \dot{m}_{34}$	$\dot{m}_{17}h_{17} + \dot{m}_{33}h_{33} = \dot{m}_1h_1 + \dot{m}_{34}h_{34} \dot{m}_{17}ex_{17} + \dot{m}_{33}ex_{33} = \dot{m}_1ex_1 + \dot{m}_{34}ex_{34} + \dot{I}_{KC,SG}$
KC Tu	$\dot{m}_1 = \dot{m}_2$	$\dot{m}_1h_1 = \dot{m}_2h_2 + \dot{W}_{KC,Tu} \dot{m}_1ex_1 = \dot{m}_2ex_2 + \dot{W}_{KC,Tu} + \dot{I}_{KC,Tu}$
KC Re1	$\dot{m}_2 + \dot{m}_{16} = \dot{m}_{17} + \dot{m}_3$	$\dot{m}_2h_2 + \dot{m}_{16}h_{16} = \dot{m}_{17}h_{17} + \dot{m}_3h_3 \dot{m}_2ex_2 + \dot{m}_{16}ex_{16} = \dot{m}_{17}ex_{17} + \dot{m}_3ex_3 + \dot{I}_{KC,Re1}$
KC MX1	$\dot{m}_4 + \dot{m}_{13} = \dot{m}_5$	$\dot{m}_4h_4 + \dot{m}_{13}h_{13} = \dot{m}_5h_5 \dot{m}_4ex_4 + \dot{m}_{13}ex_{13} = \dot{m}_5ex_5 + \dot{I}_{KC,MX1}$
KC CD1	$\dot{m}_5 + \dot{m}_{KC,CD1} = \dot{m}_6 + \dot{m}_{KC,CD1}$	$\dot{m}_5h_5 + \dot{m}_{KC,CD1}h_{cold,in} = \dot{m}_6h_6 + \dot{m}_{KC,CD1}h_{cold,out}$ $\dot{m}_5ex_5 + \dot{m}_{KC,CD1}ex_{cold,in} = \dot{m}_6ex_6 + \dot{m}_{KC,CD1}ex_{cold,out} + \dot{I}_{KC,CD1}$
KC Pu1	$\dot{m}_6 = \dot{m}_7$	$\dot{m}_6h_6 + \dot{W}_{KC,Pu1} = \dot{m}_7h_7 \dot{m}_6ex_6 + \dot{W}_{KC,Pu1} = \dot{m}_7ex_7 + \dot{I}_{KC,Pu1}$
KC F	$\dot{m}_{10} = \dot{m}_{11} + \dot{m}_{12}$	$\dot{m}_{10}h_{10} = \dot{m}_{11}h_{11} + \dot{m}_{12}h_{12} \dot{m}_{10}ex_{10} = \dot{m}_{11}ex_{11} + \dot{m}_{12}ex_{12} + \dot{I}_{KC,F}$
KC TV	$\dot{m}_{12} = \dot{m}_{13}$	$\dot{m}_{12}h_{12} = \dot{m}_{13}h_{13} \dot{m}_{12}ex_{12} = \dot{m}_{13}ex_{13} + \dot{I}_{KC,TV}$
VCR EV	$\dot{m}_{31} + \dot{m}_{36} = \dot{m}_{37} + \dot{m}_{24}$	$\dot{m}_{31}h_{31} + \dot{m}_{36}h_{36} = \dot{m}_{37}h_{37} + \dot{m}_{24}h_{24} \dot{m}_{31}ex_{31} + \dot{m}_{36}ex_{36} = \dot{m}_{37}ex_{37} + \dot{m}_{24}ex_{24} + \dot{I}_{VCR,EV}$
VCR C1	$\dot{m}_{24} = \dot{m}_{25}$	$\dot{m}_{24}h_{24} + \dot{W}_{VCR,C1} = \dot{m}_{25}h_{25} \dot{m}_{24}ex_{24} + \dot{W}_{VCR,C1} = \dot{m}_{25}ex_{25} + \dot{I}_{VCR,C1}$

$$\dot{Q}_{EV} = \dot{m}_{hf} (h_{air,out}^{EV} - h_{air,in}^{EV}) \tag{10}$$

$$\dot{W}_C = \dot{m}_{wf} (h_{wf,in}^C - h_{wf,out}^C) \tag{11}$$

The overall energy efficiency of the three cycles working together is equal to the net power generated and the heat transfer rate in the VCR evaporator divided by the total energy change of the hot fluid in the KC and ORC steam generators, as shown in Eqs. (12) and (13) [38].

$$\eta_{cyc} = \frac{\dot{W}_{net,cyc} + \dot{Q}_{EV}}{\dot{Q}_{in,cyc}} \tag{12}$$

$$\dot{W}_{net,cyc} = \dot{W}_{net,KC} + \dot{W}_{net,ORC} - \dot{W}_C \tag{13}$$

The pinch point temperature difference is the minimum temperature difference between the hot and cold fluid in heat exchangers. For pure working fluids, the temperature increases or decreases linearly, and their phase changes at a constant temperature. In contrast, for a mixture of water and ammonia, the difference in the temperature when the heat is transferred to or from the fluid is not linear. Also, the phase-changing process does not happen isothermally. Hence, it is important to pinpoint the exact location of the pinch point in the heat exchangers that use a mixture of water and ammonia or any other zeotropic mixture [41, 42]. This needs to apply the discretization method, which means dividing each heat exchanger into finite Sects. (50 segments in this study) and conducting the energy balance in each section. When the pinch point is located, the violation of its minimum temperature difference limit can

be checked. The following equations adapted from [43] are applied to perform the stated discretization method:

$$\dot{Q}_{j,sec} = \dot{Q}/sec \tag{14}$$

$$\dot{Q}_{j;j+1} = \dot{m}(h_j(T_j) - h_{j+1}(T_{j+1})) \tag{15}$$

The current paper conducts an exergy analysis to provide helpful insight into the proposed system. The exergy of a material stream includes four different terms: kinetic, potential, chemical, and physical exergies [44, 45]. In this paper, as the general assumptions stated before, the first two terms are neglected. However, since the separation and mixing process in the Kalina cycle, the ammonia concentration in the mixture, thus the chemical exergy, can vary from one stream to another [46]. Thus, the exergy of a material stream of the system is obtained by Eq. (16), which consists of physical and chemical parts of exergy as defined by Eqs. (17) and (18). Equation (19) is used to obtain the chemical exergy of the water-ammonia mixture (streams 1–17) [18].

$$\dot{E}_i = \dot{m}_i \times ex_i \tag{16}$$

$$ex_i = ex_i^{ph} + ex_i^{ch} \tag{17}$$

$$ex_i^{ph} = (h_i - h_{i,0}) - T_0(s_i - s_{i,0}) \tag{18}$$

$$ex_i^{ch} = \left(\frac{x}{M_{NH_3}}\right) \overline{ex}_{ch,NH_3}^0 + \left(\frac{1-x}{M_{H_2O}}\right) \overline{ex}_{ch,H_2O}^0 \tag{19}$$

The subscripts i and 0 indicate the number of each state and the ambient conditions, respectively. $\bar{e}_{NH_3}^0$ and $\bar{e}_{H_2O}^0$ denote the standard molar chemical exergy of ammonia and water, equal to 337.9 and 0.9 kJ/mol, respectively [47]. As mentioned, since the chemical exergy only varies within the water-ammonia mixture (and not other streams), for a more straightforward calculation, the chemical exergy of other streams is not required to be found. Hence, this parameter is only calculated for streams 1–17.

Equation (20) shows the exergy balance for each component. This equation shows that for each component, the sum of inlet exergies equals the sum of outlet exergies and exergy destruction, which originated as entropy generation.

$$\sum \dot{m}_{in} e_{in} + \dot{E}_Q = \sum \dot{m}_{out} e_{out} + \dot{E}_W + \dot{I} \tag{20}$$

\dot{E}_Q and \dot{E}_W represent the exergy rate of heat and power, respectively. \dot{I} is the exergy destruction that represents the irreversibility of the component. Table 3 shows the energy and exergy balances for components of the system. Exergy balances can be used to calculate the exergy destruction rate within each component. However, to avoid a crowded table, the repeated components (such as pumps, mixers, or condensers) are only reported once.

The ratio of product exergy to the fuel exergy of the system is defined as Eq. (21). For the KC and the ORC cycles, the exergy of the product is the net produced power, and the exergy of fuel relates to the exergy rate recovered by exhaust gas in the cycles, as written in Eqs. (22) and (23) [48]. Since the exhaust gas components remain the same within the heat recovery process, only its physical exergy needs to be taken into account.

$$\epsilon_{KC,ORC} = \frac{\dot{E}_P^{KC,ORC}}{\dot{E}_F^{KC,ORC}} \tag{21}$$

$$\dot{E}_P^{KC,ORC} = \dot{E}_W^{KC,ORC} = \dot{W}_{net}^{KC,ORC} \tag{22}$$

$$\dot{E}_F^{KC,ORC} = \dot{m}_{hf} \left(\left(h_{hf,in}^{SG} - h_{hf,0} \right) - T_0 \left(s_{hf,in}^{SG} - s_{hf,0} \right) \right) \tag{23}$$

Moreover, the exergetic COP of the VCR cycle can be obtained from the following equation, and it is defined as an exergy rise in the inlet air to the evaporator divided by the required work in the compressors.

$$COP_{ex} = \frac{E_{air,out}^{EV} - E_{air,in}^{EV}}{\dot{W}_C} \tag{24}$$

Finally, for the three cycles working integrated, it is assumed that the fuel exergy is the exergy change in the

exhaust gas throughout the two steam generators. Also, the exergy of the product is the net produced power and the change of exergy in the cooling air conditioning. Equations (25) and (23) are used to obtain this parameter.

$$\epsilon_{cyc} = \frac{\dot{E}_{P,cyc}}{\dot{E}_{F,cyc}} \tag{25}$$

$$\dot{E}_{P,cyc} = \dot{W}_{net,cyc} + E_{air,out}^{EV} - E_{air,in}^{EV} \tag{26}$$

The logic algorithm of the simulation code is presented in Fig. 2. As it is shown, the simulation algorithm tries to optimize the cycle from the thermodynamic viewpoint, which maximizes the generated power. The decision variables are X_{10} , T_{10} , and P_2 for the Kalina cycle [35]. Also, there are three other parameters that need to be solved in an iterative manner to guarantee that the pinch point rule is not violated within the heat exchangers. These parameters are T_{17} and T_{15} and T_{23} . In this study, for a faster solution, these two parameters are selected as decision variables as well. Hence, they will be found using the optimization program in a way shorter time. The validity of this modification will be seen in the validation section later.

The optimization method used in this study is *fmincon* function of the MATLAB optimization toolbox. This solver tries to solve the constrained optimization problems. The main constraints in this problem are the pinch point criteria within the heat exchangers discussed earlier and the stream quality in the turbine outlet. So, the optimization code starts from some input parameters and decision variables, then continues to simulate the cycles and calculate all state points' thermophysical properties. Also, the constraints are checked simultaneously.

After each iteration, the results are checked, and when the objective function reaches the global maximum, the solver stops. Next, these results are used to carry out the exergy, economic, and environmental assessments.

3.2 Economic analysis

The economic evaluation is performed to understand the systems' practicality better. Thermo-economic analysis can combine thermodynamics and economics by employing the Second Law of Thermodynamics [45]. However, such an assessment does not give information regarding the system's economic feasibility. As a result, a techno-economic analysis is also undertaken to evaluate a system from a more significant and applicable perspective. It takes actual economic characteristics into account when calculating words like present money value and payback period.

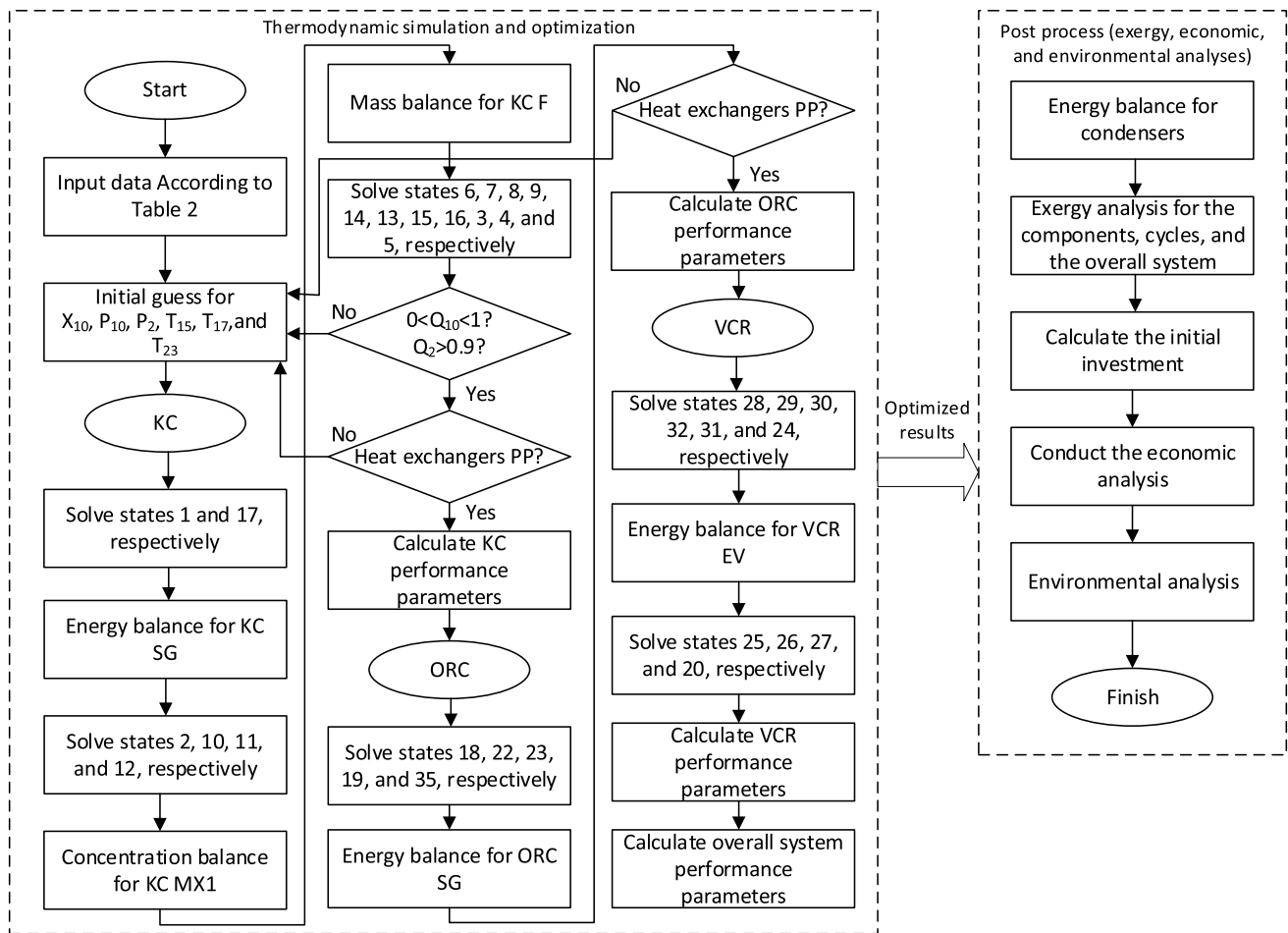


Fig. 2 Flowchart of the methodology

In this section, first, a thermo-economic analysis is formulated to calculate the cost price of the generated electricity (LCOE). Then, a techno-economic approach is introduced that contains more insightful indices, such as NPV and payback period. Conducting both these analyses can help to determine their differences. Thermo-economic assessment usually deals with the cost of the system’s product, while techno-economic assessment evaluates its economic performance in a specific market. For the current paper’s economic analysis, it is assumed that no loan or subsidy has been obtained. A cost balance can be calculated for any component as follows [49]:

$$\dot{C}_P = \dot{C}_F + \sum (\dot{C}_{Cl} + \dot{C}_{OM})_k \tag{27}$$

$$\dot{C}_F = c_F \dot{E}_F \tag{28}$$

In Eq. (27), \dot{C}_P and \dot{C}_F denote the rates of product and fuel costs (in \$/h), respectively. c_F is the unit cost of the fuel exergy (in \$/kWh_{ex}). In the overall system, containing the KC, ORC, and VCR cycles, the fuel stream is the exhaust gas stream at the entrance of the steam generator of KC (stream 33). All expenses related to the discharge of exhaust gas into the environment are already considered in the cost balances for producing electricity in the diesel engine. As a result, it is reasonable to conclude that the exhaust gases emitted by the diesel engine have no economic value when it enters the proposed system. Hence, for the proposed configuration of cycles, coupled with the exhaust gas of a diesel engine as the heat source, c_F , and subsequently, \dot{C}_F is considered zero.

Moreover, $\dot{C}_{Cl,k}$ and $\dot{C}_{OM,k}$ indicate the rates of capital investment cost and operation and maintenance cost (in \$/h) for kth component, respectively. The sum of these two terms for the overall system is estimated as follows [44]:

Table 4 Component cost functions of the system

Component	Cost Functions
Pump	$C_{CI,Pu} = 1120(\dot{W}_{Pu})^{0.8}$
Compressor	$C_{CI,C} = 44.71\dot{m}_{wf} \left(\frac{1}{0.95-\eta_{i,c}} \right) C_r \ln(C_r)$
Turbine	$C_{CI,T} = 6000(\dot{W}_T)^{0.7}$
Electrical Generator	$C_{CI,G} = 10^6 \times 10 \times \left(\frac{\dot{W}_G}{160 \times 10^3} \right)^{0.7}$
Throttling Valve	$C_{CI,TV} = 114.5\dot{m}_{wf}$
Heat Exchangers	$C_{CI,HX} = Y_1 \left(\frac{A_{HX}}{Y_2} \right)^{Y_3}, A_{HX} = \frac{\dot{Q}}{U\Delta T_{ln}}$

Table 5 Heat exchanger cost functions Coefficients

Heat Exchanger	Y_1 (\$)	Y_2 (m ²)	Y_3	U (kW/m ² K)
KC SG [54, 55]	17,500	100	0.6	1.6
ORC SG [54]	17,500	100	0.6	0.9
KC Re [55, 56]	12,000	100	0.6	1
KC Cd [55, 56]	8000	100	0.6	1.1
ORC and VCR Cd [55, 56]	8000	100	0.6	0.65
VCR EV [54]	16,000	100	0.6	1.5

$$\sum (\dot{C}_{CI} + \dot{C}_{OM})_k = \frac{TCI \times CRF \times \phi}{\tau} \tag{29}$$

In this study, the annual operation and maintenance costs are considered as 3% of the Fixed Capital Investment (FCI). So, the factor ϕ is equal to 1.03 [50]. Moreover, τ is the system’s annual operating hrs, which is considered 8000 h.

The capital recovery factor (CRF) is a ratio to calculate the present value of successive payments over a fixed amount of time. Its value can be estimated using Eq. (30) [44].

$$CRF = \frac{[i(1+i)^n]}{[(1+i)^n - 1]} \tag{30}$$

Here, i is the interest rate and is assumed to be 8%, and n represents the project lifetime, which is considered 20 years [50].

In Eq. (29), TCI is the total capital investment obtained by the sum of the purchased equipment costs (PEC) and other costs such as investments for startup, land, labor, and contingencies. They are usually expressed as a percentage of the PEC. According to the information provided in [32], the overall mentioned costs can be considered equal to 43% of the PEC, as shown in Eq. (31):

$$TCI = 1.43 \times PEC_{tot} \tag{31}$$

$$PEC_{tot} = C_{CI,SG} + C_{CI,Re} + C_{CI,EV} + C_{CI,CD} + C_{CI,TV} + C_{CI,Pu} + C_{CI,T} + C_{CI,C} + C_{CI,G} \tag{32}$$

where PEC_{tot} is the total purchased equipment cost, which is defined as the sum of the capital investment cost of system components. As seen, the costs associated with the flash separators and mixing chambers are neglected due to their relatively negligible cost compared to the other components. The capital investment cost of the compressor, pump, turbine, and generator is commonly defined as a function of the consumed or produced power in kW, as given in Table 4. The cost function of the turbine and the pump is acquired from [51], while this function for the compressor and the generator is obtained from [52] and [53].

$C_{CI,k}$ is the cost of investment for the k th component (in \$). The cost of a heat exchanger depends remarkably on the area of the heat transfer surface (A_{HX}) and the phase of fluids that are exchanging heat. For instance, the cost of a heat exchanger rises when the phase change process is to happen within it.

The heat transfer rate can be designed using the heat transfer coefficient, the total area, and the logarithmic mean temperature difference (ΔT_{ln}). In this system, Counter flow heat exchangers are considered. For obtaining ΔT_{ln} in the LMTD method, Eq. (33) can be applied.

$$\Delta T_{ln} = \frac{(T_{hf,in} - T_{cf,out}) - (T_{hf,out} - T_{cf,in})}{\ln[(T_{hf,in} - T_{cf,out}) / (T_{hf,out} - T_{cf,in})]} \tag{33}$$

The values of Y_1 , Y_2 , and Y_3 are presented in Table 5 for different heat exchangers used in the proposed structure.

The overall cost of the system consists of a summation of the purchase equipment costs for each component.

The levelized cost of energy (LCOE) in \$/GJ, also known as the levelized cost of electricity, is a quantity used to evaluate and compare alternative energy generation methods. LCOE is expressed as the average total cost of capital investment and operating and maintenance costs. It is the cost rate per unit of total electricity generated over a specified lifetime and is estimated in Eq. (34).

$$LCOE = \frac{\dot{C}_P}{\dot{W}_{net,KC} + \dot{W}_{net,ORC}} \tag{34}$$

In addition to thermo-economic analysis, there are other meaningful economic methods, such as the net present value (NPV). The NPV is a popular economic measure that shows the present value of all costs and benefits cash flows over the plant’s lifetime. The following equation is used to determine this parameter.

Table 6 validation results compared to the base reference

Modi and Haglind [35]	P_2 (bar)	x_{10}	η (%)	Calculation time (mins)
	6.04	0.6795	31.46	~ 50
This study (KC)	6.05	0.6780	31.39	~ 5
Relative difference (%)	0.17	- 0.22	- 0.22	90
Chys et al. [61]	P_{cond} (bar)	P_{eva} (bar)	\dot{W}_{net} (kW)	η (%)
	0.7	6.4	114.1	11.55
This study (ORC)	0.7	6.4	114.2	11.55
Relative difference (%)	0.00%	0.00%	0.09%	0.00%
Saleh [62]		\dot{Q}_{eva} (kW)		COP
		136.3		4.84
This study (VCR)		136.6		4.86
Relative difference (%)		0.22		0.41

$$NPV = -TCI + \sum_{t=1}^n \frac{AP}{(1+i)^t} \tag{35}$$

$$MOIC = \frac{\sum_{t=1}^n \frac{AP}{(1+i)^t}}{TCI} \tag{39}$$

n and i are the plant’s lifetime and nominal interest rate, respectively. AP is the plant’s annual benefit and can be obtained by Eq. (36) [50].

$$AP = ((\dot{W}_{net} \times \tau \times c_{se}) - (C_{OM})) \tag{36}$$

c_{se} is the unit price of electricity that is sold to the grid and is considered 0.1 \$/kWh (or 10 cent/kWh) [32]. Equation (36) shows that the plant’s annual benefit is obtained by subtracting the current annual outgoings from the yearly sales of power.

Other economic metrics, such as discounted (dynamic) pay-back period (DPP), the internal rate of return (IRR), and multiple of invested capital (MOIC) can be estimated to quantify the profitability proposed system. DPP is the time it will take for a project to “break-even.” In other terms, it is the amount of time required for the NPV to reach zero. The IRR introduces a discount rate that results in a zero NPV after the lifetime operation of the system. Equations (37)–(39) can be used to calculate DPP, IRR, and MOIC values [57]. To find the value of IRR, the iterative method should be applied since it cannot be found using direct calculations.

$$DPP = \frac{\ln\left(\frac{TCI \times (-i)}{AP} + 1\right)}{\ln\left(\frac{1}{1+i}\right)} \tag{37}$$

$$0 = -TCI + \sum_{t=1}^n \frac{AP}{(1+IRR)^t} \tag{38}$$

3.3 Environmental analysis

In addition to thermodynamic and economic assessment of the systems, environmental issues are highly important today. Environmental assessments are also important for systems that provide a way to reduce emissions of air pollutants and conserve fuels. According to Ref. [58], increased carbon dioxide emission in a system that works based on waste heat recovery is equal to the carbon dioxide that would have been emitted if the generated power from waste heat recovery was to be produced by the gas turbine or diesel engine. Based on mass analysis of the exhaust gas, the considered diesel engine produces 0.051 kg/s carbon dioxide when it produces 320 kW of power. Hence it can be concluded that to produce one kW of power using this engine, 1.61×10^{-4} kg of carbon dioxide will be released into the atmosphere. Moreover, the required fuel in this diesel engine is calculated as 0.261 L/kWh [59]. Finally, the values of avoided carbon dioxide and saved fuel are calculated using Eqs. (40) and (41), respectively [60].

$$CO_{2,AV} = 1.61 \times 10^{-4} \times (\dot{W}_{net,KC} + \dot{W}_{net,ORC}) \tag{40}$$

$$fuel_{AV} = 0.261 \times (\dot{W}_{net,KC} + \dot{W}_{net,ORC}) \tag{41}$$

Table 7 Thermodynamic properties of combined cycle state points

stream	x	m (kg/s)	T (C)	P (bar)	h (kJ/kg)	s (kJ/kg.K)	ex^{ph} (kJ/kg)	ex^{ch} (kJ/kg)
1	0.80	0.095	480.00	140	2840.49	6.95	1117.91	15,911.18
2	0.80	0.095	175.71	6.67	2169.75	7.23	362.47	15,911.18
3	0.80	0.095	96.24	6.67	1673.95	5.95	253.39	15,911.18
4	0.80	0.095	42.82	6.67	1048.34	4.14	179.22	15,911.18
5	0.68	0.153	46.77	6.67	717.76	3.08	125.21	13,542.90
6	0.68	0.153	27.02	6.67	149.78	1.23	116.79	13,542.90
7	0.68	0.153	27.08	9.00	150.22	1.23	117.09	13,542.90
8	0.68	0.058	27.08	9.00	150.22	1.23	117.09	13,542.90
9	0.68	0.095	27.08	9.00	150.22	1.23	117.09	13,542.90
10	0.68	0.095	58.55	9.00	775.84	3.20	145.10	13,542.90
11	0.99	0.036	58.55	9.00	1731.55	6.17	313.94	19,720.29
12	0.49	0.058	58.55	9.00	181.63	1.36	39.38	9702.16
13	0.49	0.058	50.33	6.67	181.63	1.36	38.49	9702.16
14	0.80	0.095	37.27	9.00	756.47	3.13	191.35	15,911.18
15	0.80	0.095	29.97	9.00	275.52	1.56	186.80	15,911.18
16	0.80	0.095	34.03	152.17	305.13	1.59	207.53	15,911.18
17	0.80	0.095	130.24	152.17	799.83	2.99	277.05	15,911.18
18	–	0.101	130.24	43.00	476.62	1.79	86.62	–
19	–	0.101	55.16	7.06	441.68	1.81	45.93	–
20	–	0.234	53.35	7.06	439.89	1.80	45.79	–
21	–	0.234	27.00	7.06	237.40	1.13	46.72	–
22	–	0.101	27.00	7.06	237.40	1.13	46.72	–
23	–	0.101	29.91	43.00	241.69	1.13	49.69	–
24	–	0.115	–8.00	1.78	395.05	1.75	15.75	–
25	–	0.115	27.75	4.00	421.15	1.78	32.49	–
26	–	0.133	25.25	4.00	418.85	1.77	32.51	–
27	–	0.133	51.98	7.06	438.53	1.80	45.70	–
28	–	0.133	27.00	7.06	237.40	1.13	46.72	–
29	–	0.133	8.93	4.00	237.40	1.13	45.62	–
30	–	0.115	8.93	4.00	212.11	1.04	47.50	–
31	–	0.115	–13.00	1.78	212.11	1.05	45.94	–
32	–	0.018	8.93	4.00	403.72	1.72	33.19	–
33	–	0.447	529.20	1.01	971.30	7.63	227.19	–
34	–	0.447	140.24	1.01	539.83	6.90	17.57	–
35	–	0.447	90.00	1.01	486.82	6.76	6.00	–
36	–	3.000	4.00	1.01	401.18	3.78	1.19	–
37	–	3.000	–3.00	1.01	394.14	3.75	1.95	–

4 Results and discussion

To ensure the validity of the results presented in this study, the ability of the developed MATLAB code to generate the results of a similar study, a simple KC12 from [35], is tested. The same inputs as the reference paper were chosen to simulate the system and conduct the simulation. As shown in Table 6, the energy efficiency and some operating parameters are compared to validate the results. There is a good fit between the results of the study and the base reference.

The results of the thermodynamic, economic, and environmental analyses will be shown in this section. Table 7 contains thermophysical properties of combined cycle state points, as shown in a schematic figure in Fig. 1. The cycle works based on the initial working condition referred to in Table 2. Since the chemical exergy is only important in the streams with a non-Constant composition, this value is only reported for the water-ammonia mixture, and it is neglected for the other streams.

Table 8 Thermodynamic results of the combined cycle based on the working condition referred to in Table 2

Parameter	Value	Unit
$\dot{W}_{net,KC}$	58.05	kW
$\dot{W}_{net,ORC}$	2.95	kW
$\dot{W}_{C,VCR}$	5.63	kW
$\dot{Q}_{Ev,VCR}$	21.12	kW
$\dot{W}_{net,cyc}$	55.37	kW
\dot{Q}_{in}^{KC}	192.86	kW
\dot{Q}_{in}^{ORC}	23.68	kW
\dot{Q}_{in}^{cyc}	216.54	kW
\dot{E}_F^{KC}	93.70	kW
\dot{E}_F^{ORC}	5.17	kW
\dot{E}_F^{cyc}	98.87	kW
η_{KC}	30.1	%
η_{ORC}	12.46	%
COP_{VCR}	3.75	-
η_{cyc}	35.32	%
$E_{D,cyc}$	41.6	kW
ϵ_{KC}	61.95	%
ϵ_{ORC}	57.11	%
$COP_{ex,VCR}$	0.62	-
ϵ_{cyc}	58.31	%

Table 9 Techno-Economic results of the combined cycle based on the working condition referred to in Table 2

Parameter	Value	Unit
PEC	180.76	k\$
TCI	258.49	k\$
\dot{C}	27.12	M\$/year
LCOE	6.12	\$/kWh
NPV	100.30	k\$
PP	10.84	year
MOIC	1.71	-
IRR	12.41	%

Table 10 Environmental results of the combined cycle based on the working condition referred to in Table 2

Parameter	Value	Unit
$CO_{2,AV}$	15.92	kg/hr
$Fuel_{AV}$	35.27	l/hr

The complete results of the thermodynamic assessment are presented in Table 8. As seen, The Kalina cycle can produce 58 kW of power from the waste exhaust gas of the diesel engine. This value is escalated by 3 kW that is generated in the ORC. This shows that coupling Kalina and organic Rankine cycles to a diesel engine that produces 320 kW power can generate 60 kW more power (18.8%) without combusting any fuel. Moreover, the VCR system demands 5.6 kW of electricity to fulfill the refrigeration demand. The energy efficiencies of the KC and ORC are

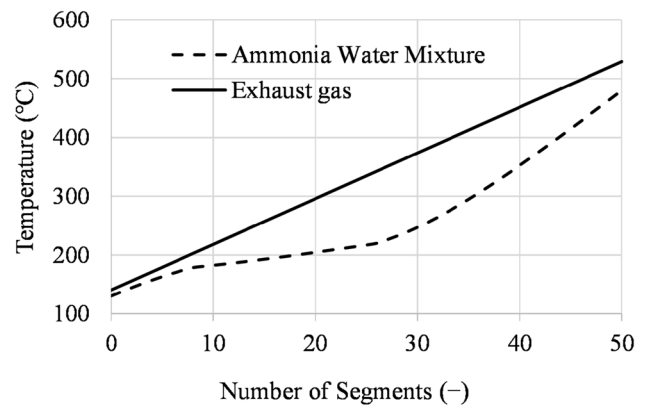


Fig. 3 Temperature profile of the Kalina steam generator

30.1% and 12.5%, respectively. Also, the VCR has a coefficient of performance equal to 3.8, and the overall system reveals an energy efficiency equal to 35.3%.

As the results of the exergy analysis show, 41.6 kW exergy is destructed due to the irreversibilities that occur within the entire system. Furthermore, the exergy efficiencies of the KC and the ORC and the exergetic COP of the VCR are 62%, 57.1%, and 0.6, respectively. The exergy efficiency of the combined cycle is 58.31%, which is quite acceptable for an energy conversion system.

Table 9 lists the results of the economic assessment. The project needs 258.5 thousand dollars as the total capital investment. Additionally, to generate one kWh of electricity in this combined cycle, \$0.06 (6.12 cents) needs to be invested, as the LCOE suggests. With the aid of the techno-economic assessment, it is revealed that after 20 years of operation, the net present value of the system is equal to 100.3 thousand dollars. Also, the invested money is returned in 10.8 years.

Finally, the results of the environmental assessment, as shown in Table 10, indicate that integrating the proposed structure with the mentioned diesel engine saves diesel fuel at a rate of 15.92 l/hr. Thus, the emission of 35.3 kg of carbon dioxide per h can be prevented.

As mentioned before, every heat exchanger in the system is considered with a minimum accepted pinch temperature limitation. In heat exchangers that use water and ammonia mixtures, the pinch point may occur within the component, so its location must be found accurately. In Fig. 3, the temperature profile of the Kalina steam generator is drawn. The horizontal axis indicates the number of the investigated nod. The nonlinear profile is an obvious behavior of the Ammonia-Water mixture in all Kalina cycles, which is clearly shown in the mentioned figure.

In Fig. 4a, b, exergy destruction of each component in the Kalina and ORC-VCR sections is presented, respectively. The highest destruction values belong to the steam generator,

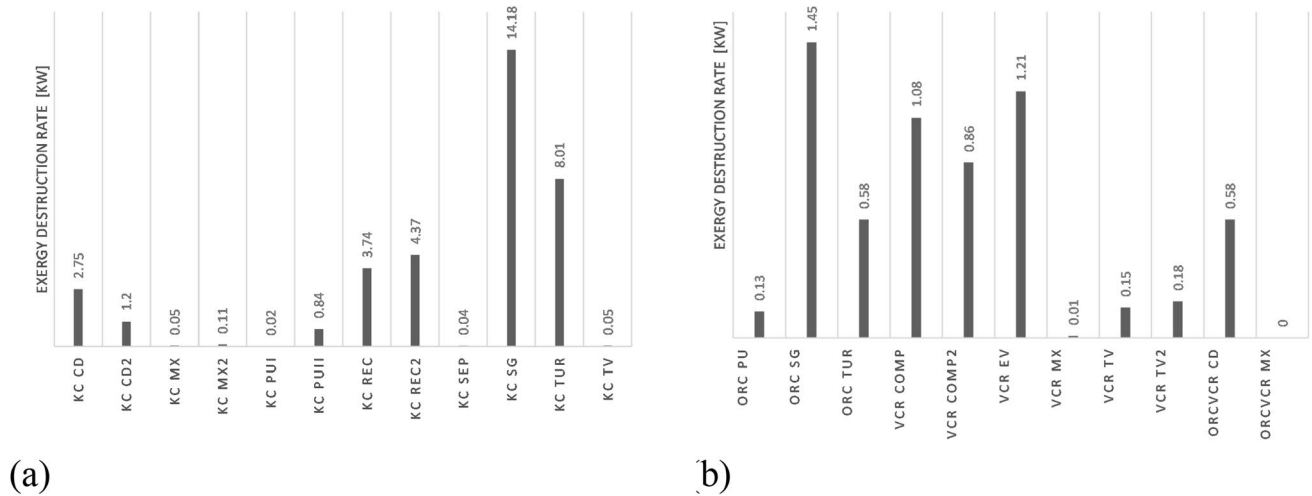


Fig. 4 Component exergy destruction rate of a Kalina section and b ORC-VCR section

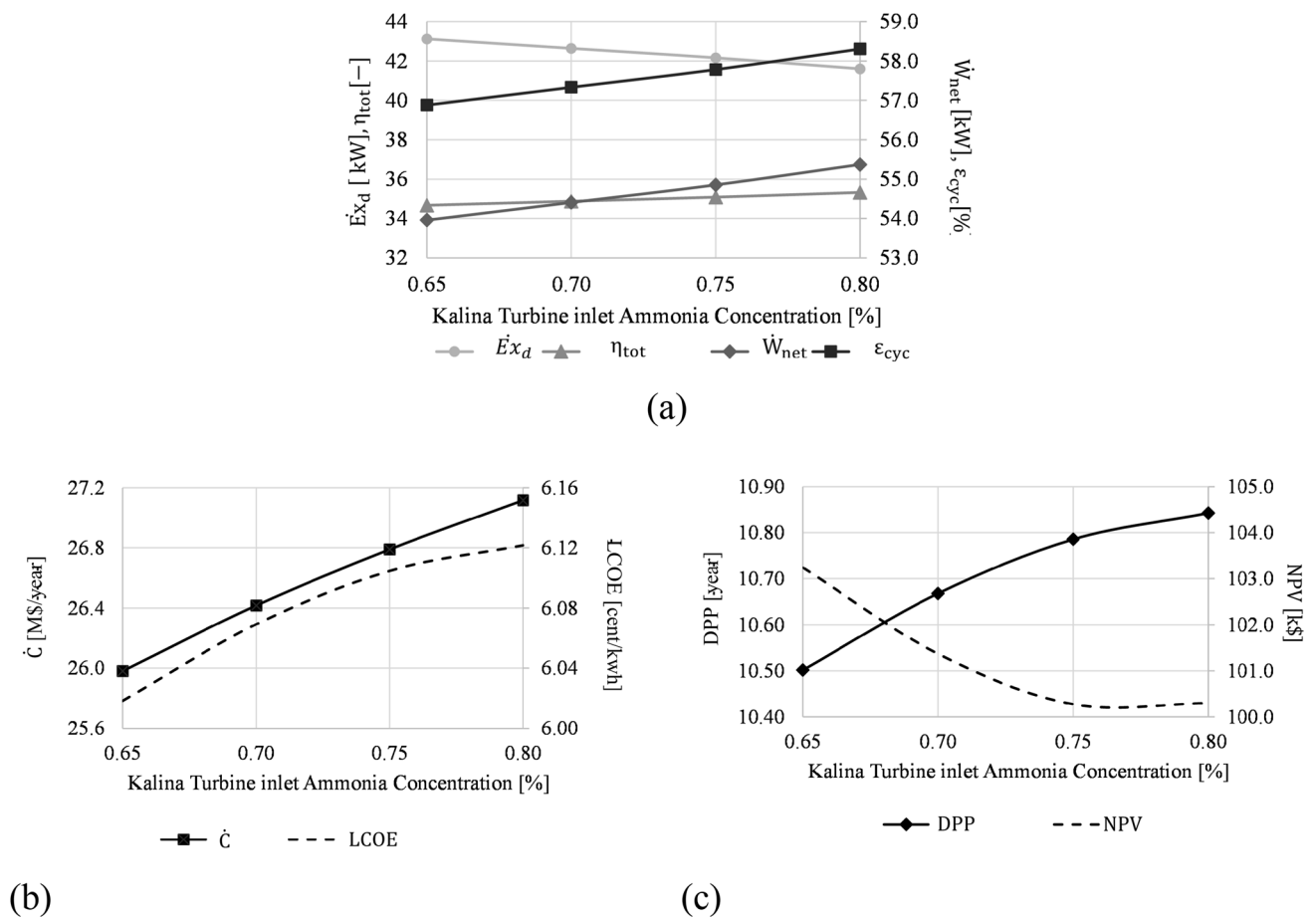


Fig. 5 Parameters variation versus Kalina turbine inlet ammonia concentration a: Overall generated power, energy, and exergy efficiencies, b: \dot{C} , LCOE, (c) : PP, NPV

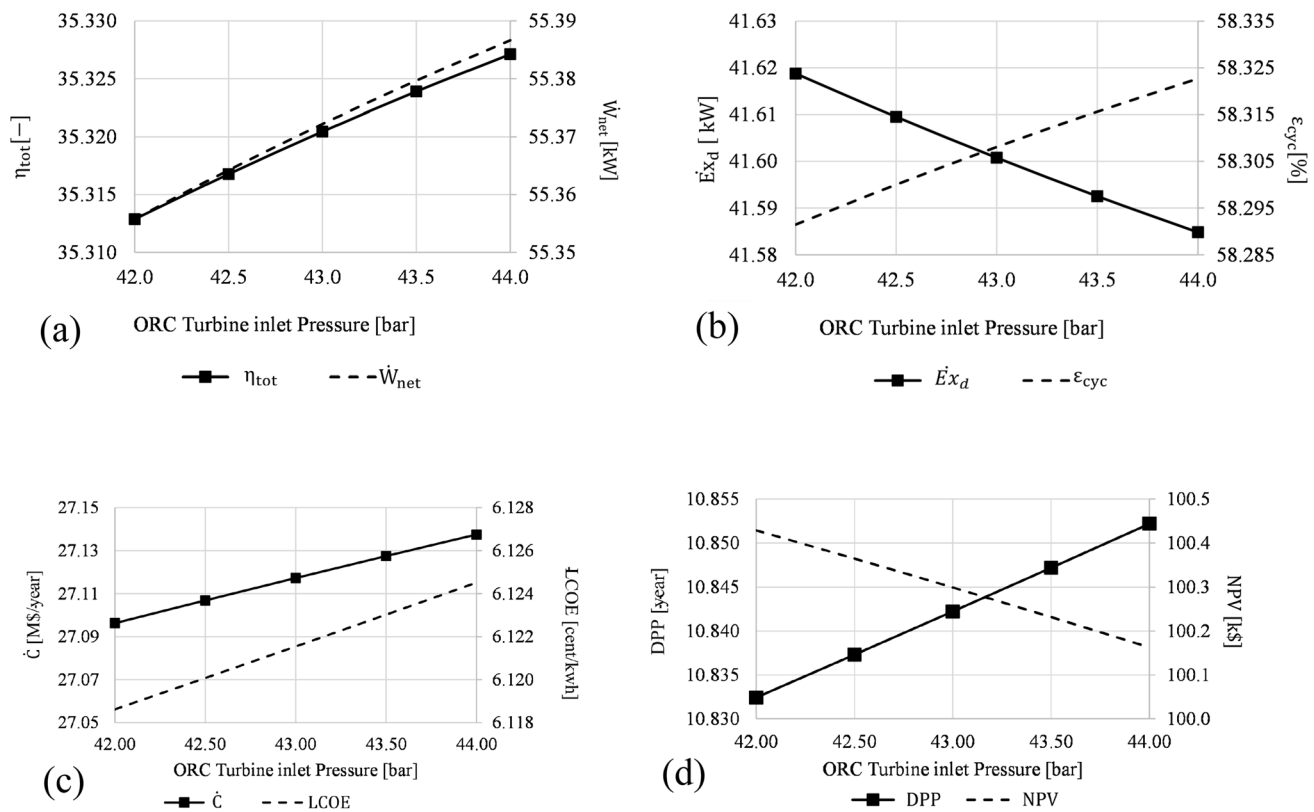


Fig. 6 Parameters variation versus inlet Pressure of ORC turbine a: Total power production, energy, and exergy efficiencies, b: \dot{C} , LCOE, PP, NPV

the Kalina turbine, and the Kalina second recuperator, with 14.18 kW, 8.01 kW, and 4.37 kW exergy destruction rates, respectively. Between the ORC-VCR components, the ORC steam generator destroyed the highest exergy amount. As seen, irreversibilities in the ORC-VCR system are not comparable with those in the Kalina cycle. This is because the Kalina cycle works at a relatively high temperature and, accordingly, produces much more power. In the ORC-VCR sub-system, the heat exchangers, including the ORC SG and the VCR evaporator, cause the most exergy destruction within the mentioned system, followed by compressors and the turbine.

In the parametric study, five parameters are considered to investigate, and their effects on the results have been studied. The investigated parameters include the ammonia concentration of the Kalina turbine inlet, the inlet pressure of the ORC turbine, the VCR flash pressure, and the inlet temperature of cooling air. The effects of the mentioned parameters are shown on produced power, energy efficiency, and exergy destruction as thermodynamic results, and total cost rate, LCOE, NPV, Payback period, internal rate of return, and multiple of invested capital, as the economic results.

Figure 5 shows the variation of the results when the ammonia concentration in the turbine inlet increases from

0.65 to 0.8. With more ammonia mass fraction at the inlet of the turbine, there will be more molar mass flow rate to the turbine. As a result, the power production, as well as the energy efficiency of the Kalina cycle, will escalate by 2.62% and 1.88%, respectively, while Exergy destruction decreases by 3.5%, as shown in Fig. 5a. As shown in Fig. 5b, c for the economic parameters, the total cost rate, LCOE, and period payback PP increased by 4.4%, 1.7%, and 3.24%. Thus, the NPV of the system declines by 2.85%. However, when the ammonia mass fraction reaches 0.8, the NPV tends to increase because its value depends on the total capital investment and the annual profit simultaneously. Here, the value of the TCI, which has a minus sign in Eq. (40), increases more; therefore, the NPV will decrease.

In Fig. 6a–d, the results versus the inlet pressure of the ORC turbine are shown. Higher pressure leads to higher power production, energy efficiency, and lower exergy destruction. Subsequently, a higher cost rate, LCOE, NPV, and lower MOIC is expected. With increasing the inlet pressure, the enthalpy of stream 18 increases, which results in higher turbine power production and higher ORC pump work. However, increasing turbine power production dominates the increasing pump work, resulting in a higher net

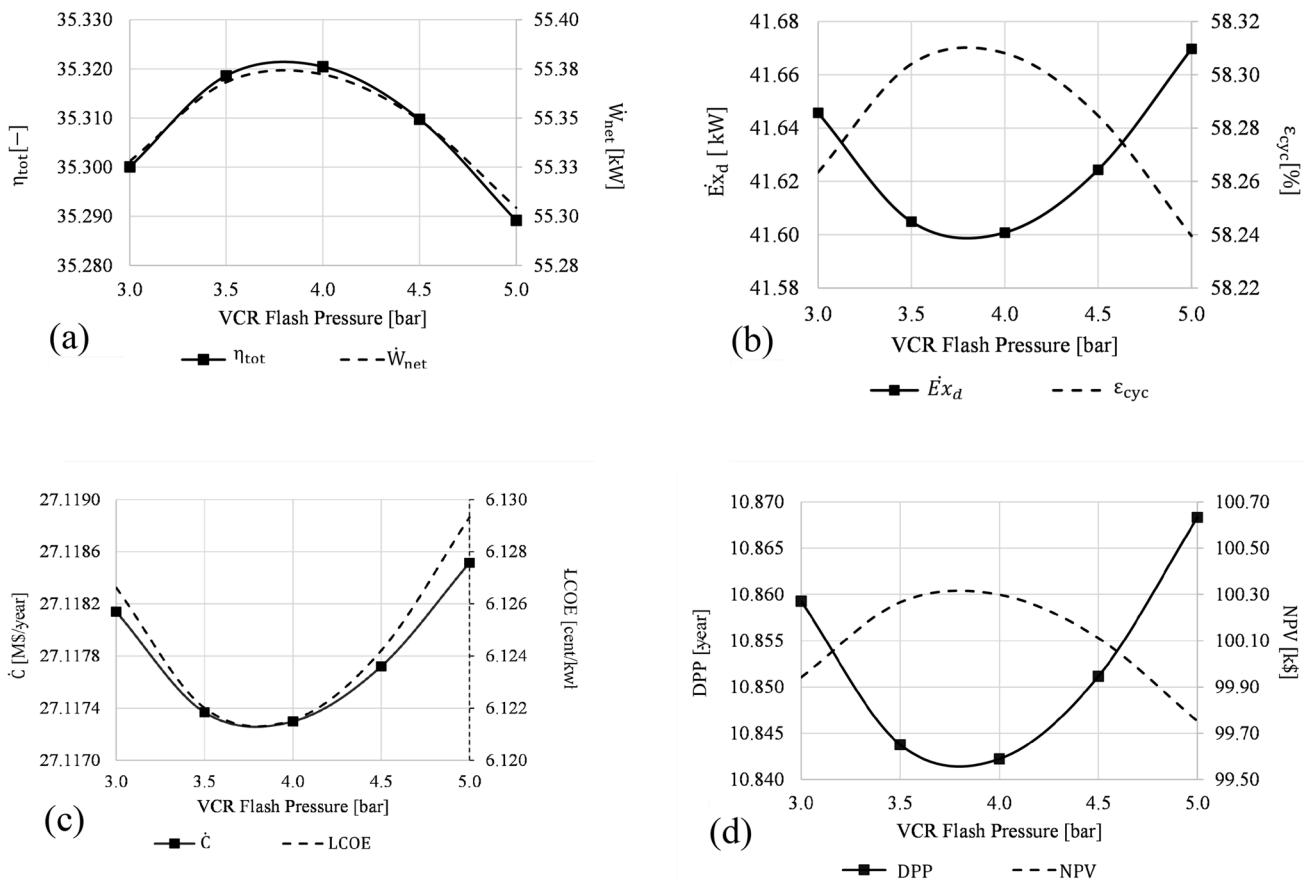


Fig. 7 Parameters variation versus Pressure of VCR Flash Chamber a: Total power production, energy, and exergy efficiencies, b: \dot{C} , LCOE, PP, NPV

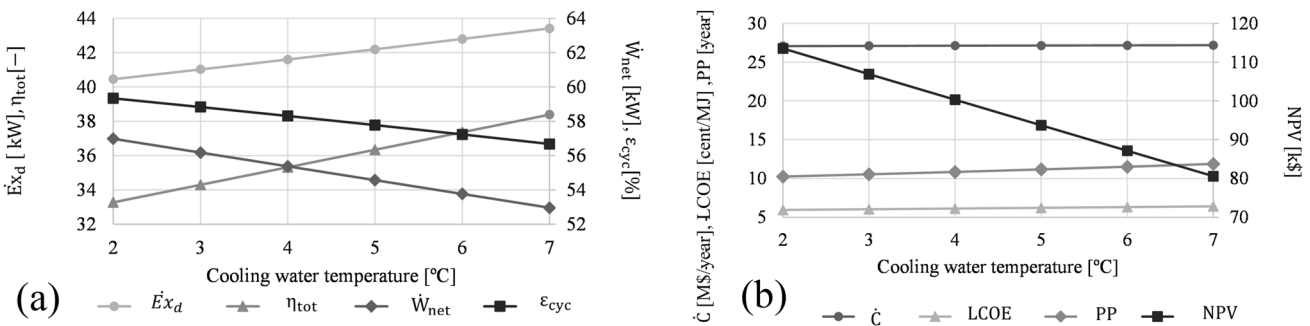


Fig. 8 Parameters variation versus Pressure of VCR Flash Chamber (a): Total power production, energy and exergy efficiencies, (b): \dot{C} , LCOE, PP, NPV

power production within the ORC. Moreover, energy efficiency increases as net power production escalates. It also leads to lower exergy destruction, which is shown in Fig. 6a, b. Due to the direct relationship between the total cost rate and power production, the total cost rate will increase with higher ORC turbine inlet pressures. In addition, as referred into Eq. (40), the value of the LCOE depends on the total capital investment and net power production. Increased

total cost rate and increased net power production cause an elevated LCOE, as revealed in Fig. 6c. The payback period increases slightly as the ORC turbine inlet pressure rises while the net present value drops, as presented in Fig. 6d.

The effects of the increasing VCR flash pressure on the results are depicted in Fig. 7. Escalating VCR flash pressure means consuming more power in the low-pressure compressor and less power in the high-pressure compressor because

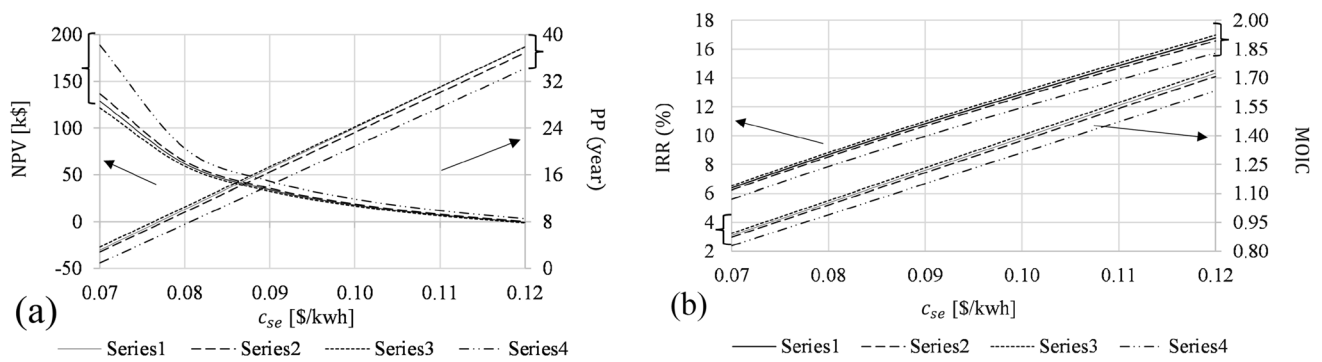


Fig. 9 Variation of **a** NPV, PP, **b** IRR, and MOCI versus variation of the unit cost of electricity for four different sets of working conditions: series 1: Base set, series 2: Base set with $P_1 = 120$, series 3: Base set with $x_1 = 0.7$, series 4: Base set with $T_{36} = 7^\circ\text{C}$

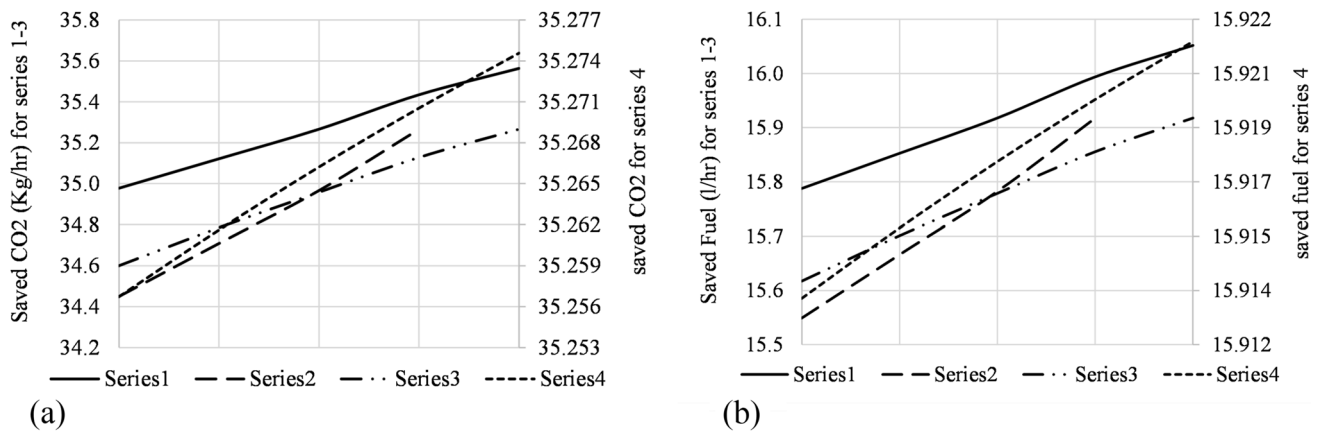


Fig. 10 Variation of fuel reduction **a** and CO₂ reduction **b** for different working conditions: series 1: Base set with varying $T_1 : 470 - 490^\circ\text{C}$, series 2: Base set with varying $X_1 : 0.65 - 0.8$,

series 3: Base set with varying $P_1 : 120 - 140\text{bar}$, series 4: Base set with varying $P_{18} : 42 - 44\text{bar}$. Carbon dioxide for the base diesel engine is 0.051 kg/s (or 183 kg/hr) for 320 kW

the more working fluid will flow through the low-pressure compressor and lower flow through the high-pressure compressor. As seen in Fig. 7a, the net power of the cycle first increases following a decline. Because the consumed power of the compressors in the VCR system first decreases and then increases. Energy and exergy efficiencies and exergy destruction will vary in the same way, as shown in Fig. 7a, b. On the other hand, the total cost rate is shown in a decreasing trend first and then increasing, as shown in Fig. 7c. It is because of the mass flow rate flowing inside the compressors. The high-pressure compressor will take a lower mass flow rate, and based on the component cost rate, the total cost rate for that compressor goes lower, while for the other compressor, the situation is inversed. The mass flow rate flows to the lower-pressure compressor goes higher, so the total cost will be increased. Until a specific pressure, the higher-pressure compressor's cost is dominant, but after a while, the other compressor's cost changes the trend of the total cost rate. As seen, it decreased first and then increased. In addition, LCOE has a similar trend to the total cost rate.

The reason is that LCOE depends on the product cost in which the total cost rate contains and produced work of the system. The product cost goes lower and then higher, as explained previously about the total cost rate.

On the other hand, work production in the correlation of LCOE is in the denominator and goes higher first and then lower. Overall, their effect on LCOE is a trend of decreasing first and then increasing. DPP and NPV are shown in Fig. 7d. Both depend on annual profit and TCI based on their correlations (34) and (36). The annual profit itself depends on the work production and operating and maintenance costs. The first one is explained before. The latter is a portion of the total cost rate. Therefore, it will show the same curvature. Based on the correlation of annual profit, the parameters made AP to be increased first and then decreased because the work production's variation dominates. DPP depends on TCI and AP. The variations of both parameters made DPP decrease first and then increase because of decreased-increased TCI and AP. AP is in the denominator in the correlation of DPP, which means it will have a reversed effect

compared to the TCI. Also, the NPV first increases and then decreases as VCR flash pressure is boosted because NPV is related to AP minus TCI, but with the dominance of AP, NPV shows a similar trend with AP.

Cooling air variation and its effect on the results are presented in Fig. 8. Lowering the temperature of evaporator cooling air means less heat transfer is required. It will decrease the consumed power in the compressor, which leads to more net power production, and escalates it by 7.59%. In addition, exergy destruction decreases by 6.8% with decreasing the cooling air temperature. An interesting result is the different trends that energy and exergy efficiencies have as the temperature of the inlet air to the VCR evaporator decreases. Here, energy efficiency increases while exergy efficiency lessens. This difference clearly shows the role of the quality of the energy, which is taken into account in the exergy analysis. Finally, due to higher power production, the total cost rate ascends, as well as LCOE and PP, by 0.4%, 7.44%, and 13.74%, respectively. Conversely, the NPV rises significantly with lowering the evaporator cooling temperature.

Also, as an important parameter, the unit cost of electricity is investigated in the parametric analysis. Its value varies from 0.06 to 0.15 €/kWh in European countries [63], and has a direct effect on the project profitability under different conditions. Therefore, an analysis is performed to investigate the sensitivity of the economic parameters while the unit cost of electricity varies from 0.07 \$/kWh to 0.12 \$/kWh. From what is presented in Fig. 9, it is revealed that the NPV decreases with an increase in the unit cost of electricity while DPP, IRR, and MOIC increase. The reason is that AP is defined by the unit cost of electricity. When the unit cost goes higher, AP will be increased. With higher AP, NPV, IRR, and MOIC will go higher based on their correlations defined previously. While DPP will be decreased as AP has an inverse effect on DPP's amount based on correlation (36). It is obvious that with higher annual profit, the capital investment will be back to the investor in a shorter time.

The results of the environmental assessment are shown in Fig. 10a, b. Saved fuel and the prevented CO₂ release are calculated using Eqs. (45) and (46). As presented, in each series, a parameter changes, which leads to more fuel savings and, therefore, results in less CO₂ emitted to the environment. According to the mentioned equations, there is a direct relationship between the saved fuel and the generated power in the cycle. The same trend is seen for the prevented carbon dioxide emission.

5 Conclusions

A new combined Kalina-ORC-VCR cycle is proposed to fully recover the waste heat from the diesel engine C13 ACERT-DE400E0. Energy, exergy, and thermo-economic analyses are applied to calculate the net power production, energy and exergy efficiencies, exergy destruction, and economic results, including the total cost rate, the levelized cost of electricity, the net present value, and the dynamic payback period. To perform the thermo-economic analysis, cost functions are considered for the components, which are formulated based on the calculation of the heat transfer area of all heat exchangers. Also, the exergy destruction rates of all components are calculated, showing which components should be improved. A parametric study shows how the calculated parameters change with variation of working parameters, including Kalina turbine inlet ammonia concentration, ORC turbine inlet pressure, VCR flash pressure, cooling water temperature, and as an effective economic parameter, unit cost of electricity. In addition, an important environmental result of utilizing this combined system to recover the waste heat is investigated by calculating saved fuel and saved CO₂ pollution. The 4E analyses represent that coupling a bottoming Kalina-ORC-VCR system to the diesel engine produces 60 kW more power (18.8%) with no fuel consumption. However, the Kalina cycle has a higher share in producing extra power compared to the ORC one. With 41.6 kW exergy destruction, the combined cycle has 58.31% exergy efficiency. Also, an economic investigation reveals that 258.5 thousand dollars are needed to invest in the project, which will return after 10.8 years. Also, an additional 6.12 cents will be required to produce 1 kWh of electricity in this system. Finally, from the environmental analysis, it is concluded that 15.92 l/hr of diesel fuel is saved, which means 35.3 kg of carbon dioxide per h is not emitted into the atmosphere.

With all the benefits of such a system that is discussed in this work, there are aspects that can be further assessed in future research works. A dynamic assessment based on working hrs, especially for the cooling system, can be the objective of the next research. Also, a more detailed environmental analysis that takes different pollutants into account is another interesting area for upcoming assessments.

Acknowledgements The authors would like to thank the Research Institute of Applied Power System Studies, Azarbaijan Shahid Madani University, for partially supporting this study.

Author contributions Supervision, Conceptualization, Writing-Review & Editing (M. F); Formal Analysis, Writing-Original Draft, Validation, coding (AS); Validation, coding, Literature review, Plots extraction and interpretation, Review & Editing (NH. M).

Declarations

Conflict of interest All authors certify that they have no affiliations with or involvement in any organization or entity with any financial or non-financial interest in the subject matter or materials discussed in this manuscript.

References

- IPCC. Assessment Report 6 Climate Change 2021: The Physical Science Basis 2021.
- Shu G, Liu L, Tian H, Wei H, Yu G (2014) Parametric and working fluid analysis of a dual-loop organic rankine cycle (DORC) used in engine waste heat recovery. *Appl Energy* 113:1188–1198. <https://doi.org/10.1016/j.apenergy.2013.08.027>
- Keinath CM, Delahanty JC, Garimella S, Garrabrant MA (2022) Compact diesel engine waste-heat-driven ammonia-water absorption heat pump modeling and performance maximization strategies. *J Energy Res Technol, Transact ASME*. <https://doi.org/10.1115/1.4051804/1114649>
- Shu G, Liang Y, Wei H, Tian H, Zhao J, Liu L (2013) A review of waste heat recovery on two-stroke IC engine aboard ships. *Renew Sustain Energy Rev* 19:385–401. <https://doi.org/10.1016/j.rser.2012.11.034>
- Yu SC, Chen L, Zhao Y, Li HX, Zhang XR (2015) A brief review study of various thermodynamic cycles for high temperature power generation systems. *Energy Convers Manag* 94:68–83. <https://doi.org/10.1016/j.enconman.2015.01.034>
- Omar A, Saghafifar M, Mohammadi K, Alashkar A, Gadalla M (2019) A review of unconventional bottoming cycles for waste heat recovery: Part II – applications. *Energy Convers Manag* 180:559–583. <https://doi.org/10.1016/j.enconman.2018.10.088>
- Roge NH, Khankari G, Karmakar S (2022) Waste heat recovery from fly ash of 210 MW coal fired power plant using organic rankine cycle. *J Energy Resour Technol*. 10(1115/1):4052949
- Kalina AI, Leibowitz HM, President V, Systems A. (1988) The Design of a 3MW Kalina Cycle Experimental Plant .
- Wang J, Dai Y, Gao L (2009) Exergy analyses and parametric optimizations for different cogeneration power plants in cement industry. *Appl Energy* 86:941–948. <https://doi.org/10.1016/j.apenergy.2008.09.001>
- Butrymowicz D, Gagan J, Łukaszuk M, Śmierciew K, Pawluczuk A, Zieliński T et al (2021) Experimental validation of new approach for waste heat recovery from combustion engine for cooling and heating demands from combustion engine for maritime applications. *J Clean Prod*. <https://doi.org/10.1016/j.jclepro.2020.125206>
- Ouyang T, Huang G, Lu Y, Liu B, Hu X (2021) Multi-criteria assessment and optimization of waste heat recovery for large marine diesel engines. *J Clean Prod* 309:127307. <https://doi.org/10.1016/j.jclepro.2021.127307>
- Ouyang T, Huang G, Su Z, Xu J, Zhou F, Chen N (2020) Design and optimisation of an advanced waste heat cascade utilisation system for a large marine diesel engine. *J Clean Prod* 273:123057. <https://doi.org/10.1016/j.jclepro.2020.123057>
- Bo Z, Mihardjo LW, Dahari M, Abo-Khalil AG, Al-Qawasmi AR, Mohamed AM et al (2021) Thermodynamic and exergoeconomic analyses and optimization of an auxiliary tri-generation system for a ship utilizing exhaust gases from its engine. *J Clean Prod* 287:125012. <https://doi.org/10.1016/j.jclepro.2020.125012>
- Singh OK, Kaushik SC (2013) Thermoeconomic evaluation and optimization of a Brayton-Rankine-Kalina combined triple power cycle. *Energy Convers Manag* 71:32–42. <https://doi.org/10.1016/j.enconman.2013.03.017>
- Bombarda P, Invernizzi CM, Pietra C (2010) Heat recovery from diesel engines: a thermodynamic comparison between Kalina and ORC cycles. *Appl Therm Eng* 30:212–219
- Feng Y, Du Z, Shreka M, Zhu Y, Zhou S, Zhang W (2020) Thermodynamic analysis and performance optimization of the supercritical carbon dioxide Brayton cycle combined with the Kalina cycle for waste heat recovery from a marine low-speed diesel engine. *Energy Convers Manag* 206:112483. <https://doi.org/10.1016/j.enconman.2020.112483>
- Hua J, Li G, Chen Y, Zhao X, Li Q (2015) Optimization of thermal parameters of boiler in triple-pressure Kalina cycle for waste heat recovery. *Appl Therm Eng* 91:1026–1031. <https://doi.org/10.1016/j.applthermaleng.2015.09.005>
- Mohammadkhani F, Yari M, Ranjbar F (2019) A zero-dimensional model for simulation of a Diesel engine and exergoeconomic analysis of waste heat recovery from its exhaust and coolant employing a high-temperature Kalina cycle. *Energy Convers Manag* 198:111782. <https://doi.org/10.1016/j.enconman.2019.111782>
- Baldi F, Gabrielli C (2015) A feasibility analysis of waste heat recovery systems for marine applications. *Energy* 80:654–665. <https://doi.org/10.1016/j.energy.2014.12.020>
- Larsen U, Van NT, Knudsen T, Haglind F (2014) System analysis and optimisation of a Kalina split-cycle for waste heat recovery on large marine diesel engines. *Energy* 64:484–494. <https://doi.org/10.1016/j.energy.2013.10.069>
- Jannatkhah J, Najafi B, Ghaebi H (2021) Energy and exergy analysis of combined ORC – ERC system for biodiesel-fed diesel engine waste heat recovery. *Energy Convers Manag*. <https://doi.org/10.1016/j.enconman.2020.112658>
- Liu X, Quang Nguyen M, He M (2020) Performance analysis and optimization of an electricity-cooling cogeneration system for waste heat recovery of marine engine. *Energy Convers Manag*. <https://doi.org/10.1016/j.enconman.2020.112887>
- Liang Y, Sun Z, Dong M, Lu J, Yu Z (2020) Investigation of a refrigeration system based on combined supercritical CO₂ power and transcritical CO₂ refrigeration cycles by waste heat recovery of engine. *Int J Refrig* 118:470–482. <https://doi.org/10.1016/j.ijrefrig.2020.04.031>
- Zhi LH, Hu P, Chen LX, Zhao G (2020) Performance analysis and optimization of engine waste heat recovery with an improved transcritical-subcritical parallel organic Rankine cycle based on zeotropic mixtures. *Appl Therm Eng*. <https://doi.org/10.1016/j.applthermaleng.2020.115991>
- Ding P, Yuan Z, Shen H, Qi H, Yuan Y, Wang X et al (2020) Exergoeconomic analysis and optimization of a hybrid Kalina and humidification-dehumidification system for waste heat recovery of low-temperature Diesel engine. *Desalination*. <https://doi.org/10.1016/j.desal.2020.114725>
- Liu X, Nguyen MQ, Chu J, Lan T, He M (2020) A novel waste heat recovery system combining steam Rankine cycle and organic Rankine cycle for marine engine. *J Clean Prod*. <https://doi.org/10.1016/j.jclepro.2020.121502>
- Feng Y, Du Z, Shreka M, Zhu Y, Zhou S, Zhang W (2020) Thermodynamic analysis and performance optimization of the supercritical carbon dioxide Brayton cycle combined with the Kalina cycle for waste heat recovery from a marine low-speed diesel engine. *Energy Convers Manag*. <https://doi.org/10.1016/j.enconman.2020.112483>
- Hoseinzadeh S, Heyns PS (2021) Advanced energy, exergy, and environmental (3E) analyses and optimization of a coal-fired 400 MW thermal power plant. *J Energy Res Technol, Transact ASME*. <https://doi.org/10.1115/1.4048982/1089720>

29. Haq MZ (2021) Optimization of an organic rankine cycle-based waste heat recovery system using a novel target-temperature-line approach. *J Energy Res Technol*, Transact ASME., <https://doi.org/10.1115/1.4050261/1100435>
30. Lemmon E, Huber M, McLinden M. NIST Standard Reference Database 23: Reference Fluid Thermodynamic and Transport Properties-REFPROP, Version 9.1 2013.
31. <http://www.cat-electricpower.com/>. Diesel Engine retail sell: Eneria 2016.
32. Kolahi M, Yari M, Mahmoudi SMS, Mohammadkhani F (2016) Thermodynamic and economic performance improvement of ORCs through using zeotropic mixtures: case of waste heat recovery in an offshore platform. *Case Stud Therm Eng*. <https://doi.org/10.1016/j.csite.2016.05.001>
33. Hoang AT (2018) Waste heat recovery from diesel engines based on Organic Rankine Cycle. *Appl Energy* 231:138–166. <https://doi.org/10.1016/J.APENERGY.2018.09.022>
34. Banifateme M, Behbahaninia A, Sayadi S (2021) Development of a loss method for energy and exergy audit of condensing hot water boilers. *J Energy Resour Technol* 143:1–8. <https://doi.org/10.1115/1.4049415>
35. Modi A, Haglind F (2015) Thermodynamic optimisation and analysis of four Kalina cycle layouts for high temperature applications. *Appl Therm Eng* 76:196–205. <https://doi.org/10.1016/j.applthermaleng.2014.11.047>
36. Yataganbaba A, Kilicarslan A, Kurtbaş I (2015) Exergy analysis of R1234yf and R1234ze as R134a replacements in a two evaporator vapour compression refrigeration system. *Int J Refrig* 60:26–37. <https://doi.org/10.1016/j.ijrefrig.2015.08.010>
37. Köse Ö, Koç Y, Yağlı H (2020) Performance improvement of the bottoming steam Rankine cycle (SRC) and organic Rankine cycle (ORC) systems for a triple combined system using gas turbine (GT) as topping cycle. *Energy Convers Manag*. <https://doi.org/10.1016/j.enconman.2020.112745>
38. Moran MJ, Shapiro HN, Boettner DD. *Fundamentals of Engineering Thermodynamics*, 7th Edition. Wiley Global Education; 2010.
39. Lecompte S, Ameer B, Ziviani D, Van Den Broek M, De Paepe M (2014) Exergy analysis of zeotropic mixtures as working fluids in Organic Rankine Cycles. *Energy Convers Manag* 85:727–739. <https://doi.org/10.1016/J.ENCONMAN.2014.02.028>
40. Yang F, Cho H, Zhang H (2019) Performance prediction and optimization of an organic rankine cycle using back propagation neural network for diesel engine waste heat recovery. *J Energy Res Technol*, Transact ASME., <https://doi.org/10.1115/1.4042408/368475>
41. Sohrabi A, Behbahaninia A (2022) Conventional and advanced exergy and exergoeconomic assessment of an optimized system consisting of kalina and organic rankine cycles for waste heat recovery. *J Energy Resour Technol* 10(1115/1):4054178
42. Sohrabi A, Behbahaninia A, Sayadi S (2021) Thermodynamic optimization and comparative economic analysis of four organic Rankine cycle configurations with a zeotropic mixture. *Energy Convers Manag* 250:114872. <https://doi.org/10.1016/j.enconman.2021.114872>
43. Karellas S, Schuster A, Leontaritis AD (2012) Influence of supercritical ORC parameters on plate heat exchanger design. *Appl Therm Eng* 33–34:70–76. <https://doi.org/10.1016/j.applthermaleng.2011.09.013>
44. Dincer I, Rosen MA. *Exergy*. 2012.
45. Adrian Bejan, George Tsatsaronis MJM. *Thermal design and optimization*. 1996.
46. Mokarram NH, Mosaffa AH (2018) A comparative study and optimization of enhanced integrated geothermal flash and Kalina cycles: a thermoeconomic assessment. *Energy* 162:111–125. <https://doi.org/10.1016/j.energy.2018.08.041>
47. Szargut J. (2005) *Exergy Method: technical and ecological applications*. WIT Press
48. Hu S, Li J, Yang F, Yang Z, Duan Y (2020) Thermodynamic analysis of serial dual-pressure organic Rankine cycle under off-design conditions. *Energy Convers Manag*. <https://doi.org/10.1016/j.enconman.2020.112837>
49. Lazzaretto A, Tsatsaronis G (2006) SPECO: a systematic and general methodology for calculating efficiencies and costs in thermal systems. *Energy* 31:1257–1289. <https://doi.org/10.1016/j.energy.2005.03.011>
50. Georgousopoulos S, Braimakis K, Grimekis D, Karellas S (2021) Thermodynamic and techno-economic assessment of pure and zeotropic fluid ORCs for waste heat recovery in a biomass IGCC plant. *Appl Therm Eng*. <https://doi.org/10.1016/j.applthermaleng.2020.116202>
51. Shokati N, Ranjbar F, Yari M (2015) Exergoeconomic analysis and optimization of basic, dual-pressure and dual-fluid ORCs and Kalina geothermal power plants: a comparative study. *Renew Energy* 83:527–542. <https://doi.org/10.1016/J.RENENE.2015.04.069>
52. Momeni M, Jani S, Sohani A, Jani S, Rahpeyma E (2021) A high-resolution daily experimental performance evaluation of a large-scale industrial vapor-compression refrigeration system based on real-time IoT data monitoring technology. *Sustain Energy Technol Assess* 47:101427–98. <https://doi.org/10.1016/J.SETA.2021.101427>
53. Bahrapoury R, Behbahaninia A (2017) Thermodynamic optimization and thermoeconomic analysis of four double pressure Kalina cycles driven from Kalina cycle system 11. *Energy Convers Manag* 152:110–123
54. Javanshir N, Mahmoudi SMS, Rosen MA (2019) Thermodynamic and exergoeconomic analyses of a novel combined cycle comprised of vapor-compression refrigeration and organic rankine cycles. *Sustainability* 11(12):3374. <https://doi.org/10.3390/SU1123374>
55. Ding P, Yuan Z, Shen H, Qi H, Yuan Y, Wang X et al (2020) Exergoeconomic analysis and optimization of a hybrid Kalina and humidification-dehumidification system for waste heat recovery of low-temperature diesel engine. *Desalination* 496:114725. <https://doi.org/10.1016/J.DESAL.2020.114725>
56. Campos Rodríguez CE, Escobar Palacio JC, Venturini OJ, Silva Lora EE, Cobas VM, Marques Dos Santos D et al (2013) Exergetic and economic comparison of ORC and Kalina cycle for low temperature enhanced geothermal system in Brazil. *Appl Therm Eng* 52:109–19
57. Kalogirou SA. (2014) *Solar Energy Engineering: Processes and Systems: Second Edition*. Elsevier Inc. <https://doi.org/10.1016/C2011-0-07038-2>.
58. Boyaghchi FA, Molaie H (2015) Advanced exergy and environmental analyses and multi objective optimization of a real combined cycle power plant with supplementary firing using evolutionary algorithm. *Energy* 93:2267–2279. <https://doi.org/10.1016/J.ENERGY.2015.10.094>
59. RETAIL RANGE – DIESEL POWER GENERATORS FROM 9.5 TO 715 KVA n.d. <https://www.eneria.fr/en/energy/diesel-generator-sets/product-range/retail/> (accessed August 21, 2021).
60. Sohrabi A, Asgari N, Imran M, Wakil Shahzad M (2023) Comparative energy, exergy, economic, and environmental (4E) analysis and optimization of two high-temperature Kalina cycles integrated with thermoelectric generators for waste heat recovery from a diesel engine. *Energy Convers Manag* 291:117320–98. <https://doi.org/10.1016/j.enconman.2023.117320>
61. Chys M, van den Broek M, Vanslambrouck B, De Paepe M (2012) Potential of zeotropic mixtures as working fluids in organic Rankine cycles. *Energy*. <https://doi.org/10.1016/j.energy.2012.05.030>

62. Saleh B (2018) Energy and exergy analysis of an integrated organic Rankine cycle-vapor compression refrigeration system. *Appl Therm Eng* 141:697–710. <https://doi.org/10.1016/j.applthermaleng.2018.06.018>
63. Tocci L, Pal T, Pasmazoglou I, Franchetti B (2017) Small scale organic rankine cycle (ORC): a techno-economic review. *Energies (Basel)* 10:413. <https://doi.org/10.3390/en10040413>

Springer Nature or its licensor (e.g. a society or other partner) holds exclusive rights to this article under a publishing agreement with the author(s) or other rightsholder(s); author self-archiving of the accepted manuscript version of this article is solely governed by the terms of such publishing agreement and applicable law.

Publisher's Note Springer Nature remains neutral with regard to jurisdictional claims in published maps and institutional affiliations.